INTERNATIONAL JOURNAL OF AUTOMOTIVE SCIENCE AND TECHNOLOGY

2024, VOL. 8, NO: 1, 1-22 www.ijastech.org e-ISSN: 2587-0963

Computational Fluid Dynamics of Four Stroke In-Cylinder Charge Behavior at Distinct Valve Lift Opening Clearance in Spark Ignition Reciprocating Internal Combustion Renault Engine

Aniekan Essienubong Ikpe[1*] and Michael Okon Bassey[2]

[1]*Department of Mechanical Engineering Technology, School of Engineering, Akwa Ibom State Polytechnic, Ikot Osurua, PMB 1200, Nigeria*
[2]*Department of Mechanics Engineering Technology, School of Engineering, Akwa Ibom State Polytechnic, Ikot Osurua, PMB 1200, Nigeria*

Abstract

Renault internal combustion engines have complex, expensive, and challenging experimentally computed in-cylinder flow dynamics. The current study employed computational fluid dynamics to simulate the in-cylinder charge behavior at various valve lift opening clearance in a four-stroke spark-ignition internal combustion engine. The governing equations for an unstable, three-dimensional and compressible turbulent flow were computed using the continuity equations (for mass conservation), Navier-Stokes equations (for momentum conservation), and RNG k- turbulence model. The engine was modelled using SolidWorks 2019 while the in-cylinder charge behavior was simulated using ANSYS Fluent 14.5 model. The thermal characteristics and parameters with respect to air-fuel mixtures were observed to improve with higher temperature (with respect to the cylinder) during combustion. The volumetric and mechanical efficiency of the cycle significantly improved as a result of the increased valve lift opening clearance, which caused more charge to be ingested into the cylinder. Additionally, it was found that at lower valve lift, which may be characterized by minimal or zero losses, the rate of heat retention in the cylinder was at its peak, but very high cylinder charge temperatures was predisposed to a decrease in the intake charge density. From the Particle Image Velocimetry (PIV) obtained in this study, increasing valve lift opening clearance led to increase in-cylinder velocity vectors, vorticity magnitudes, and distributions of turbulence kinetic energy (TKE), which signified improvement in combustion efficiency, increased torque and power output for efficient engine performance.

Keywords: In-cylinder temperature; IC engine; Mechanical efficiency; TKE; Velocity vectors; Valve lift clearance.

Research Article

History
Received 03.08.2023
Revised 14.11.2023
Accepted 24.12.2023

Contact
* Corresponding author
Aniekan Essienubong Ikpe
aniekan.ikpe@akwai-bompoly.edu.ng
Address: Department of Mechanical Engineering Technology, School of Engineering, Akwa Ibom State Polytechnic, Ikot Osurua, Nigeria.
Tel:+2349024773812

***To cite this paper*:** Ikpe, AE., Bassey, MO., Computational Fluid Dynamics of Four Stroke In-Cylinder Charge Behavior at Distinct Valve Lift Opening Clearance in Spark Ignition Reciprocating Internal Combustion Renault Engine. International Journal of Automotive Science and Technology. 2024; 8(1):1-22. http://dx.doi.org/10.30939/ijastech..1337386

1. Introduction

Simulation of vehicle components plays a key role in automotive R&D process [1], like the in-cylinder combustion simulation which is the subject of this study. Internal Combustion Engine (ICE) analysis can be divided into three main categories: in-cylinder combustion modelling, cold flow; and port flow [2-3]. The combustion of air-fuel combination occurs in the combustion chamber of IC engines, where it reacts to produce hot gases at high temperatures and pressure, creating the torque and power needed to keep the engine operating at peak efficiency [4-5]. A complex thermochemical process known as high-temperature, high-pressure turbulent fluid dynamics is involved in the in-cylinder combustion of air-fuel mixtures in internal combustion engines (ICEs) during various engine strokes [6-7]. While computational fluid dynamics (CFD) computes the in-cylinder fluid flow behavior, heat and mass transfer, thermochemical reactions, and the mechanical behavior of the combustion cycle at various engine stokes in ICEs, numerical simulation computes turbulent mixing, fuel atomization and vaporization as well as flow visualization [8-9]. However, the governing equations of mass, momentum, and energy transport can also be used to analyze the complex behavior of fluid flow in the combustion chamber during combustion cycles [10-11].

Recent research on the behavior of the in-cylinder charge in

ICEs has shown that air flow during the intake stroke and inside the cylinder significantly affects air-fuel mixing and, consequently, the efficiency of the combustion process. Large-scale flow structures like swirl and tumble motion increase the rate of turbulence flow at the point of ignition, which improves both the emission of pollutants and fuel economy while the engine is operating [12-13]. A range of measuring and visualization techniques have been used to examine the complex unstable in-cylinder charge behavior and study in-cylinder charge behavior at different strokes, with particle image velocimetry (PIV) being one of the most prominent. The PIV technique is widely employed in experimental fluid mechanics, where instantaneous velocity vector fields are examined in connection to fluid motion. PIV measuring techniques have been used in studies of ICEs that have characterized the behavior of in-cylinder turbulent flow [14], examined the spatial flow regime in the cylinder, revealed the flow variations of the in-cylinder combustion cycle [15], and computed the flow regime during injection and ignition process [16].

El-Adawy et al. [17] conducted an experimental investigation of the in-cylinder flow behavior in ICEs under steady-state conditions using Ricardo and FEV flow benches. The trials were conducted on an identical cylinder head with a pressure differential of 600 mmH2O across the input valves in order to compare the results. Correlation between the two flow benches existed up to a 6 mm valve lift; however, at that point, the FEV flow bench began to choke, which had an effect on the values of the flow and discharge coefficients. In order to analyze the turbulent fluid flow (TFF) across the intake valve of a single-cylinder ICE represented by a magnetic resonance velocimetry (MRV) flow bench configuration with a Reynolds number of 45,000, Nishad et al. [18] used large eddy simulation (LES). A progressive increase in Turbulent Length Scale (TLS) downstream of the in-cylinder turbulent flow and intake port was suggested by streams of turbulent scales along the intake charge. A significant amount of turbulence is produced during the valve passage, which is primarily responsible for in-cylinder turbulence, according to the evolution of turbulence properties over the port length [19].

Rahiman et al. [20] developed the flow field around a direct injection diesel engine with various manifolds using ANSYS Fluent and RNG k- turbulence models. The CFD analysis used a multi-cylinder DI diesel engine with a 10 mm valve lift and 1000 rpm setting, a dynamic mesh of 0.25 million tetrahedral and hexahedral elements, and a no-slip condition on the walls. The results showed that helical intake manifolds had superior volumetric efficiency while spiral and helical-spiral intake manifolds produced larger swirl ratios.

Particle Image Velocimetry (PIV) was used by Mohammed et al. [21] to experimentally examine tumble flow structures in steady-state situations while taking into account the center vertical tumble plane. A four-valve, pent-roof gasoline DI engine head was used for the experiment, and it was run at various valve lift openings with a 150 mmHg pressure differential across the intake valves. According to the results, for valve lifts of 1 to 5 mm, the flow energy concentrated in large (mode 1) eddies between 46.6 and 48.9%, with only 8.4 to 11.46% in mode 2 and 7.2 to 7.5% in model 3. A portion of the energy in the massive eddies of mode 1 was transferred to the lesser structures of flow of modes 2 and 3 as the valve lift rose. For the 1 mm, 5 mm, 9 mm, and 10 mm valve lifts, Mode 1 included roughly 48.9%, 46.6%, 43.2%, and 40.6% of the Turbulent Kinetic Energy (TKE).

Azad et al. [22] numerical computation of the 4-cylinder E-TVCS Diesel engine's flow regime at 2400 rpm and 0.2 mm of minimum valve lift. CFD codes in ANSYS Fluent were used as the main solution for the flow. The problem was computed using the common k-turbulent model and PISO method. The results showed that swirl ratio had a substantial impact on combustion efficiency and emissions, and that the mass average TKE was higher in the air intake stroke than the exhaust stroke. Using ANSYS R-16 software, Ikpe et al. [23] performed port flow simulation in ICE at an 8 mm valve lift opening clearance. Utilizing swirl motion simulation profiles and cut planes, the magnitude of the velocity and mass flow rate were monitored. Average crankshaft angular velocity was measured to be 1315 rpm with a recorded percentage deviation of less than 20%, while area-weighted average charge velocity was 11 m/s and corresponding mass flow rate was -0.055479 kg/s. Additionally, 0.005417 kg/s was the highest flow rate that could be calculated at 8 mm. Along the engine cylinder's stroke length, a rise in swirl motion intensity was seen. Additionally, a rise in the swirl number resulted in a consistent distribution of radial temperature and a decrease in flame temperature.

The effects of intake port design and valve lift on the flow and burn rate of the in-cylinder air-fuel combination were examined by Kent et al. [24]. Two separate intake ports and four different intake valve lifts, ranging from 25% to 100% of full lift, were used to report the results. For the two ports, opposite trends in swirl vs. valve lift were seen. While burn duration reduced with increasing swirl ratio and velocity fluctuation, it was shown that velocity fluctuations were rather insensitive to changes in valve lift. Krishna et al. [25] used particle image velocimetry to examine the effects of intake manifold tilt on single-cylinder engine intake valve flow parameters. The findings indicated that engine speed and intake valve lift both enhanced turbulent kinetic energy as well as circumferential and longitudinal air velocity.

Experimental research on the turbulent structures produced by a DISI-engine's intake port was conducted by Kapitza et al. [26], Using a steady-state test bench called the tumble optical test-bench, the transient behavior of the charge through the intake port was determined. Higher in-cylinder charge variations were seen to be caused by an increase in mass flowrate, a closed tumble flap, and a decrease in valve lift. PIV approach was used by Rabault et al. [27] to investigate intake flow in a diesel engine cylinder. The findings showed that at higher valve lifts, orderly flow patterns were produced near the cylinder head while greater whirling flow patterns were seen further from the cylinder head for higher valve lifts. The cycle-to-cycle variances increased as a result of this incident, which further impacted the engine's performance.

A steady state flow bench (that directly introduces air into the cylinder) linked to a 4-valve 125 cc engine cylinder head was used by Wahono et al. [28]. The impact of two pressure differences (300 and 600 mmH_2O) across the intake valves on the in-cylinder flow

regime was measured using a torque meter. TKE, TLS, and Turbulent Kinetic Viscosity (TKV) were found to significantly increase with increased valve lift and pressure drop in both horizontal and vertical planes. Both the rate of air-fuel mixing and the rate of homogenous flame propagation increased as a result. In order to optimize fuel delivery and in-cylinder combustion performance, it is crucial to understand the process output of four-stroke internal combustion engines. However, it could be time-consuming and extremely expensive, especially if sophisticated equipment is needed for measuring, reading, and producing data for analysis [29]. The use of Computational Fluid Dynamics (CFDs) tools has recently been used for complicated study of in-cylinder charge behavior during combustion [30], even though certain data may not be accurate if the equipment is not accurately calibrated during the experimental procedure.

According to studies, there is always little to no error when comparing experimentally generated data with data produced by several common CFD tools [31]. Internal combustion (IC) engines play a crucial role in various industries, including automotive, aerospace, and power generation. The efficiency and performance of IC engines heavily rely on the design and operation of their components, such as valves. Valve lift, which refers to the maximum displacement of the valve from its seat, significantly affects engine performance and fuel consumption [32]. Despite extensive research in this field, there exists a research gap concerning the optimization of valve lift in IC engines. Existing studies have primarily focused on optimizing valve timing, neglecting the potential benefits of valve lift optimization. Most research assumes a fixed valve lift throughout the engine's operating range, disregarding the potential benefits of variable valve lift systems. Variable valve lift systems have the potential to enhance engine efficiency, power output, and emissions control. The limited research on variable valve lift systems restricts their widespread implementation in IC engines. The absence of standardized methodologies for valve lift optimization hampers the comparison and replication of research findings. Researchers employ different experimental setups, simulation models, and evaluation criteria, leading to inconsistent results. The establishment of standardized methodologies would facilitate knowledge sharing and accelerate advancements in valve lift optimization. The existing research gap in IC engine valve lift optimization highlights the need for further investigation in this area. The valve lift in IC engines plays a vital role in determining power output, fuel consumption and overall engine performance. By optimizing valve lift, engineers can achieve improved power output, reduced fuel consumption, lower emissions, and enhanced engine performance. This can provide outcomes that are comparable to those seen in real-world situations.

In this study, computational fluid dynamics of four stroke in-cylinder charge behavior was examined at distinct valve lift opening clearance in spark ignition reciprocating internal combustion Renault engine. The four-stroke spark-ignition reciprocating IC engine and its components were modelled using SOLIDWORKS 2019 while the in-cylinder charge temperature at different valve lift opening clearance, volumetric efficiency, and mechanical efficiency were simulated using ANSYS Fluent 14.5 at various engine speeds. Based on Particle Image Velocimetry, in-cylinder flow paths of the Renault engine were seen at various valve lift openings (5, 7, 10 and 13 mm).

2. Methods

The reciprocating IC engine (see Fig. 1a) has two in-line exhaust and induction valves, and the theoretical cycle's compression and expansion processes are also included in the practical cycle. The charges (air-fuel mixture) are introduced into and drained from the cylinder in this instance through ports, the opening and closing of which are correlated with the location and motion of the piston within the cylinder. But for an IC engine to operate effectively, valve timings and ignition locations are also crucial. A Spark Ignition (SI) engine's typical p-V diagram is shown in Fig. 1b. As the piston descends from Top Dead Center (TDC) to Bottom Dead Center (BDC) during the induction stroke, sometimes referred to as the first stage of the IC engine cycle, air-fuel mixture is delivered into the cylinder.

The cylinder pressure decreases to a value in the range of atmospheric pressure (760 mm Hg) as a result of the piston movement in this order. The carburetor, which also receives a measured amount of gasoline, is used to feed air through the engine as the piston that is moving downward approaches the bottom of the cylinder. After the piston has moved halfway along the return stroke, the inlet valve closes at position 2 (see Fig. 1b). Reciprocating IC engine, SI engine pressure volume diagram, and four-stroke SI engine timing diagram are shown in Fig. 1. The air-fuel combination is trapped in the cylinder and compressed by the reciprocating piston while the intake and exhaust valves are closed. As a result, the charge's volume occupied above the piston at TDC is known as the clearance volume. The charge is precisely timed to occur just before TDC at position S (see Fig. 1b). The in-cylinder combustion of the air-fuel mixture is now occurring at virtually constant volume with a noticeable rise in temperature and pressure [33]. Due to the heated, high-pressure consequence, the in-cylinder charge expands significantly, pushing the piston down into the cylinder. The expansion process is expected to end at point 4 (see Fig. 1b), but in order to improve the expulsion of combusted gaseous products, the exhaust valve opens before BDC, maybe at point E (see Fig. 1b). As the in-cylinder pressure decreases to virtually atmospheric pressure (760 mm Hg), 60% of the gas is released from the exhaust between E and 4 (see Fig. 1b), where the pressure is approximately 3.7 bar or higher [34].

The exhaust gas is cleared by the returning piston, and at this stroke, the pressure is just above atmospheric pressure. Fresh air and fuel are combined in the in-cylinder charge just prior to compression, and some exhaust gas from the previous cycle is added to dilute it [35, 36]. A typical timing diagram for a four-stroke SI engine is shown in Fig. 1c.

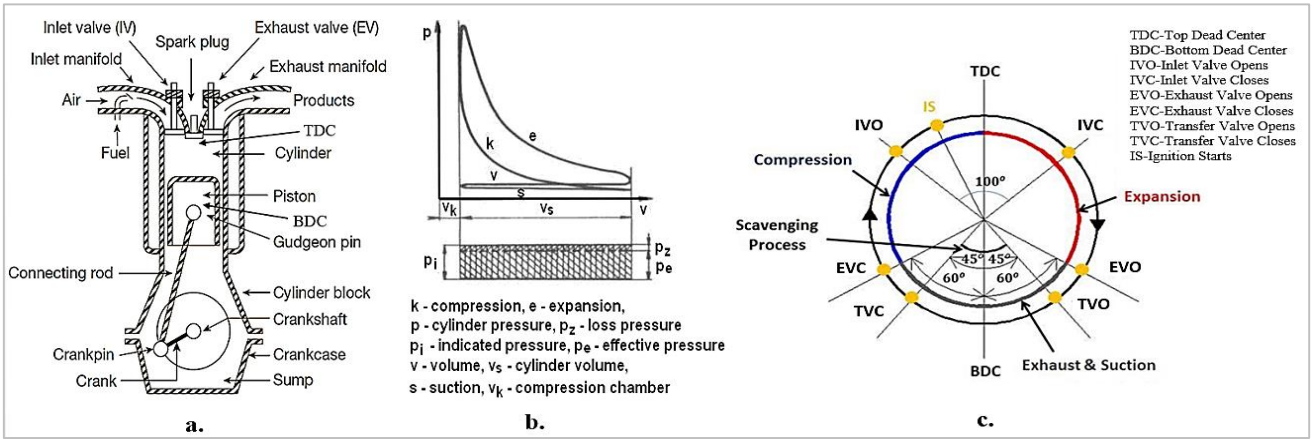

Fig. 1. a. Reciprocating IC engine, b. Pressure volume diagram for SI engine, c. Timing diagram for four-stroke SI engine

In relation to the piston's TDC and BDC positions, the angular positions in terms of crank angle are shown [34].

i. IVO Inlet valve Opens: This occurs between 10° and 15° before TDC.
ii. IVC Inlet valve Opens: In order to capitalize on the moment of the quickly flowing gas, the real position of the inlet valve is between 20º and 40º after BDC.
iii. S Spark: This occurs at TDC when ignition is totally retarded and between 20º and 40º before TDC when ignition is further advanced.
iv. EVO Exhaust valve opens: This position typically occurs 50º before BDC, however it can be higher in racing car engines.
v. EVC Exhaust valve closure: This takes place between 0o and 10o after TDC.

Calculating the volumetric and mechanical efficiency of an IC engine is crucial for optimizing its performance. By utilizing ANSYS Fluent software in this study, the following procedures were adopted to compute the volumetric and mechanical efficiency in Renault production engine (Mercedes-Benz 250SE) W108 type.

i. Geometry Creation: Creating a 3D model of the IC engine intake system. This included the engine geometry such as intake manifold, valves, and cylinder etc. as well as boundary conditions and appropriate turbulence models. Some fluid dynamic factors such as valve lift, valve timing, and port geometry were also considered.
ii. Mesh Generation: Generating a high-quality mesh that captures the intricate details of the intake system. Appropriate meshing techniques was employed such as structured or unstructured mesh, to ensure accurate representation of the flow physics. The mesh near critical regions, such as valve seats and ports was refined to capture flow phenomena accurately.
iii. Boundary Conditions: Appropriate boundary conditions for the intake system were defined. Inlet boundary conditions were specified by setting the mass flow rate or velocity profile to represent the incoming air-fuel mixture. The outlet boundary condition was set to atmospheric pressure, while also considering back pressure effects. Wall boundary conditions, including wall roughness and thermal properties were properly defined. The mass flow rate of air-fuel mixture entering the cylinder during intake stroke was also defined.
iv. Solver Settings: Appropriate solver settings were selected in the ANSYS Fluent interphase, considering the type of flow (compressible or incompressible) and turbulence model (e.g., k-ε). Convergence criteria was set for the solution in order to ensure accurate results.
v. Simulation and Post-processing: The simulation in ANSYS Fluent was initiated to solve the governing equations of fluid flow and obtain the flow field within the intake system, and compute the results for volumetric and mechanical efficiency which are presented in the results section of this paper. The combustion process was simulated using appropriate combustion models, such as the Reynolds-Averaged Navier-Stokes (RANS) equations coupled with the Flamelet Generated Manifold (FGM) approach. The simulation accounted for factors such as heat transfer, combustion efficiency, and fluid dynamics to accurately predict the mechanical efficiency.

Each valve's typical opening and closing positions are shown by the point there. Each valve will be fully open for a crank angle movement significantly less than that indicated by the timing diagram, according to the time needed to open and close the valves. The engine was modelled in SOLIDWORKS 2019 for this investigation. The experimental data was gathered at various engine speeds of a Renault production engine (Mercedes-Benz 250SE) W108 type. It is believed that the engine was a spark ignition (SI) engine and ran on a four-stroke cycle.

The engine's flywheel was built to hold any extra energy generated during the power stroke. Over the course of six seconds, the vertical displacement of the piston, power, momentum, and trace routes were evaluated. Fig. 2a-b show the front and end views of the ICE engine model, and Fig. 2c depicts the cylinder port with the intake and exhaust valves. The entire ICE model's parts (the piston head, connecting rod, flywheel, and crankshaft) are shown

in Fig. 3-6. A piston that travels in the cylinder and creates a moveable, gas-tight plug, a connecting rod, and a crank shaft make up the reciprocating engine mechanism..

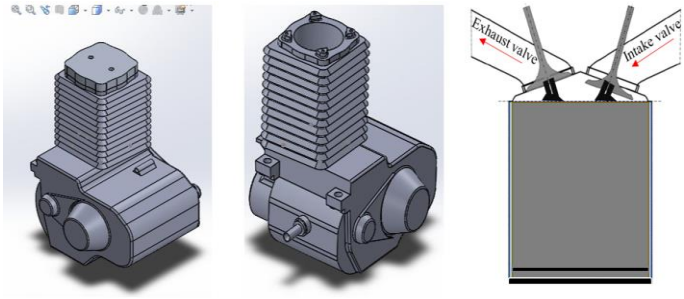

a. Engine model-Front view b. Engine model-End view c. Cylinder port and valves

Fig. 2. Engine model, cylinder port and valves

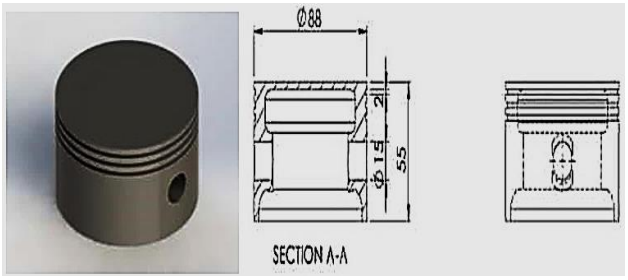

Fig. 3. IC Engine piston head assembly

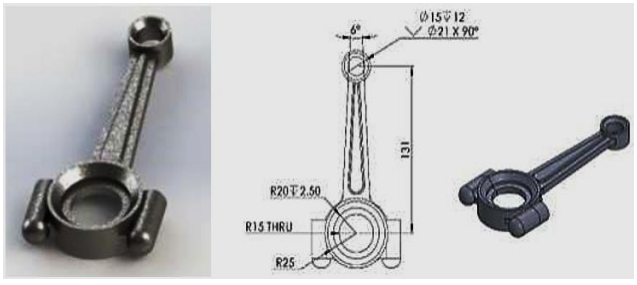

Fig. 4. Piston assembly for an IC engine

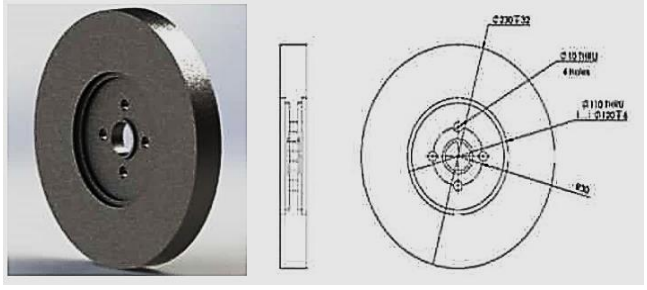

Fig. 5. Flywheel rod assembly details for an IC engine

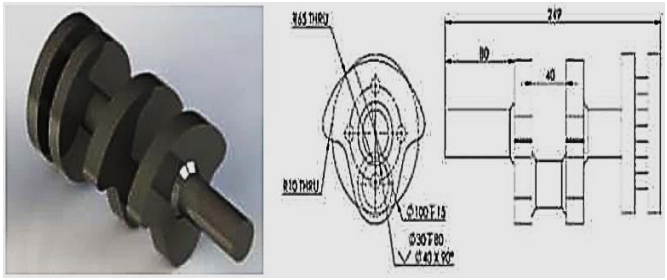

Fig. 6. Details of the IC engine crankshaft assembly

Table 1 lists the variables and boundary conditions used in the IC engine study. These were taken from a technical report on a Mercedes-Benz 250SE production engine by Renault that was designed by Ayub et al. (W108 model) [37]. Table 2 lists the boundary physics for the ICE simulation, relaxation, pressure-velocity coupling, and discretization strategy. The method of analysis and solution used to examine and resolve the internal combustion engine (ICE) in-cylinder flow was CFD in the ANSYS R-16 software, which used the finite volume method of numerical analysis to resolve the continuity, Navier-Stokes, and energy equations [38].

ANSYS Fluent 14.5 version was employed as a simulation software of choice to analyze the fluid flow, heat transfer, and other physical phenomena required in the study. To use ANSYS Fluent 14.5 version on SOLIDWORKS CAD model, the SolidWorks CAD model profile was imported into ANSYS Fluent 14.5 version as a geometry saved in initial graphics exchange specification (IGES) file format. After importation of the geometry, the simulation was initiated by defining the parametric conditions (fluid properties, boundary conditions, and other parameters required in the study). This was followed by the simulation and analysis of results to gain insights into the fluid flow and heat transfer as shown in this research study.

In ANSYS Fluent 14.5, the software generated a mesh, checked the geometry's decomposition into separate zones, and set up boundary conditions. The final step was to run a transient in-cylinder simulation, which set up and automatically generated the default swirl plane from geometry information, defined custom field functions for vorticity magnitudes, velocity vector fields, and in-cylinder TKE distributions, and provided adequate representation of the 3D streamline plots. In order to mesh the solid surface and resolve the turbulent boundary layer on the solid surface domain, triangular elements were used, while developing prismatic cells were thought to be sufficient for the valve surface. The elements chosen were both tetrahedral and hexahedral mesh volume, with a total of 0.32 million elements (0.1 million tetrahedral and 0.17 million hexahedral).

Table 1. Engine parameters and boundary conditions

Parameters of the Engine	Corresponding Values	Boundary conditions	Values
Compression Ratio	9.3:1	Initial solid temperature	293.20 K
Stroke	68mm	Pressure of air	1.65 bar
Bore	92mm	Temperature of air	301.15 K
Displacement	2500cc	Turbulent Viscosity	1.000 Ns/m^2
Con rod length	122.5	Air to fuel ratio	14.6:1
Swept volume	499.5cm^3	Static Pressure	1.00 bar
Inner seat diameter	33.7mm	Percentage fuel by mass	6.9%
Number of valves	4	Mass flow rate	0.0020 kg/s
Valve stem diameter	5.5mm	% squish area	10.8
Seat angle	45º	Specific Dissipation Rate	0.750 m^2/s^3
Range of θs	-30º to +30º with respect to TDC	Specific heat ratio	1.4
Range of θ_b	30º to 120º	Air to fuel ratio	14.6/1

Table 2. Boundary physics for the ICE simulation

Relaxation and Pressure-Velocity Coupling			
Relaxation		**Pressure-Velocity Coupling**	
Variable	Relaxation Factor	Type	Coupled
Density	1.000 kg/m^3	Pseudo Transient	yes
Body Forces	1.000	Explicit momentum under-relaxation	0.500
Turbulent Kinetic Energy	0.750 J/kg	Explicit pressure under-relaxation	0.500
Specific Dissipation Rate	0.750 m^2/s^3		
Turbulent Viscosity	1.000 $N.s/m^2$		
Energy	0.750 N.m		
Discretization Scheme			
Variable		Scheme	
Pressure		Standard	
Density		Second Order Upwind	
Momentum		Second Order Upwind	
Turbulent Kinetic Energy		First Order Upwind	
Specific Dissipation Rate		First Order Upwind	
Energy		Second Order Upwind	
Simulation Physics Parameters			
Fuel temperature (°C)		80	
Injection quality (mg)		74.28	
injection pressure (MPa)		15	
initial velocity (m/s)		150	
injection duration (ms)		4.23	
initial particle size (mm)		0.1	
computing time (ms)		5	
time step (ms)		0.05	
maximum iteration step length		100	

A unique approach for modelling ICE combustion chamber processes, ANSYS Fluent software streamlines the process of creating 3D models for combustion chambers. A portion of the input and output ducts were also modelled. The execution of all phases in semi-automatic mode, with the exception of boundary conditions, in this method enabled a significant reduction in the time required for 3D model development. The fact that all relevant options were highlighted in a separate window made this stage simpler. A minimum gap between the valve and the saddle, a crank radius, a shaft length, distortion of the crank axis in reference to the cylinder axis, and a shaft length were all established initially. The ANSYS Fluent module automatically generated a piston motion equation as well as equations for the valve motions. The 3D model was then imported into the ANSYS Fluent design modelling interface. It comprised a single model of the internal combustion chamber component and two separate models of the input and output valves. This 3D model showed the surfaces of the input and output ducts, the cylinder's surface, the input and output valves, and their saddles. Equations for valve motion were applied to related valves. A specific crank angle could either be chosen from the possibilities the

program suggests or set as the initial value. In this case, the combustion chamber is divided into 21 volumes along with portions of the input and output ducts. The combustion chamber was divided into 3 volumes, and the ducts were each divided into 9 volumes (Fig. 7a). Tetrahedral finite elements was then used to mesh two of these volumes (the head-end and the upper portion of the combustion chamber), and volumes in the shape of a triangular prism was used to mesh the volume in between them. During calculation and stacking of the mesh during piston motion, the elements around the valve were remeshed. The algorithm probably may not separate the combustion chamber into three volumes if the cylinder wall is quite thin when the piston is positioned in upper dead center. In this instance, two planes to separate the combustion chamber were selected. Before the model was separated into the volumes, the piston top and valve motion animation had initiated a pre-check command to verify that the parameters were suitable. The configuration program separated the model into volumes afterwards. For the specific non-stationary task, each volume had its unique mesh parameters. Model separation into finite elements had two standard regimes namely: coarse and fine. During mesh automated setting, they were selected. In relation to the valve diameter, these settings were parameterized. It was possible to modify both common parameters and settings for each component formed during separation if the default settings were not suitable. With the help of this tool, it was possible to visually verify which model had been divided into finite elements, for instance, in the valve symmetry plane (Fig. 7b) or in any other plane that the user created. Mesh independence refers to the state where the numerical solution of a problem remains unchanged with respect to changes in the mesh resolution.

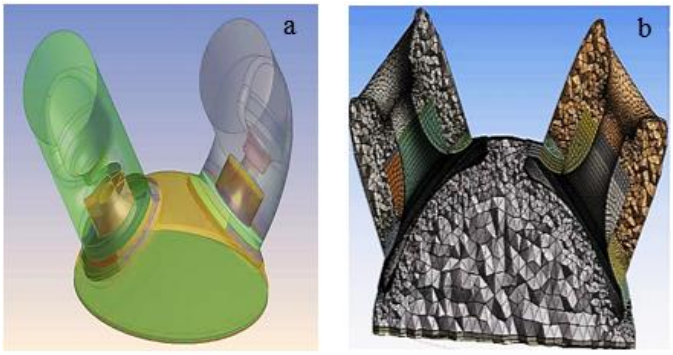

Fig. 7a. CAD model of the cylinder head, 7b. Mesh model of the cylinder head showing valve symmetry plane

In IC engine simulations, mesh independence is essential to obtain accurate and reliable results. It refers to the state where the numerical solution of a problem remains unchanged with respect to changes in the mesh resolution. Achieving mesh independence involves iteratively refining the mesh until the solution no longer changes significantly. The IC engine model was meshed consisting of 453176 nodes and 303472 elements. Employing mesh independence as the standard meshing procedure (This included: geometry preparation, mesh generation, initial simulation, mesh refinement, iterative simulations and convergence criteria) and recommended mesh quality (see Fig. 8), mesh parameters such as average element quality of 0.82, average skewness quality of 0.26, and average orthogonal quality of 0.85 were obtained. These conforms to the mesh quality criteria employed by Fatchurrohman and Chia, [39] and Adam et al. [40].

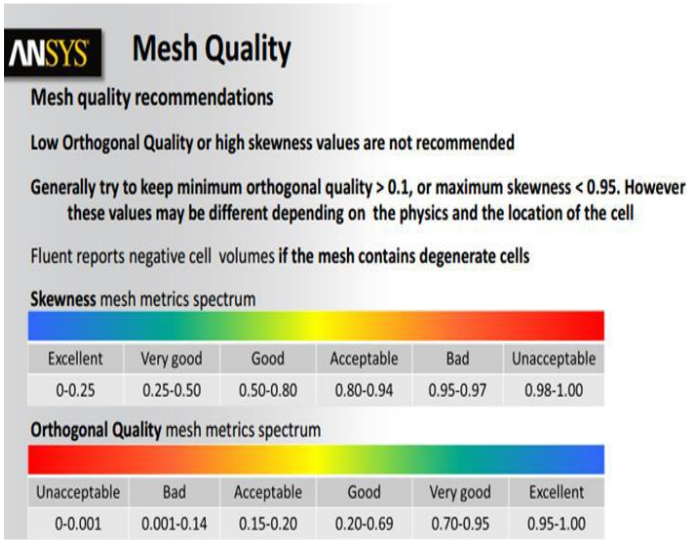

Fig. 8. Recommended mesh quality criteria

After mesh generation, solution parameter settings was performed next. The Fluent program was utilized in a certain system to extract all calculation-related applications which were then executed individually. The model was afterwards loaded into the fluent module, where computations had already begun. A narrow duct turn radius caused the area of the vortex flow, which reduced the flow of fuel-air mixture through the duct. As a corrective measure, the input duct's geometry was modified and the computation carried out a second time. A vacuum is produced as the revolving piston moves downward in the downward stroke shown in Fig. 9a, from Top Dead Center (TDC) to Bottom Dead Center (BDC). Fresh air-fuel combination enters the combustion chamber from the crankcase and fills the cylinder's vacuum at the same time. The reciprocating piston of the IC engine is depicted moving along the cylinder in Fig. 9b.

The poppet valve gradually closes as the reciprocating piston moves down the cylinder because of increased crankcase pressure development. Before the end of the stroke, the compressed air-fuel mixture in the crankcase expands, as seen in Fig. 10. The enlarged air-fuel combination can then enter the main cylinder and undergo compression and expansion at high temperatures and pressures before being discharged from the IC engine thanks to the intake port being exposed by the reciprocating piston as it approaches the end of its stroke.

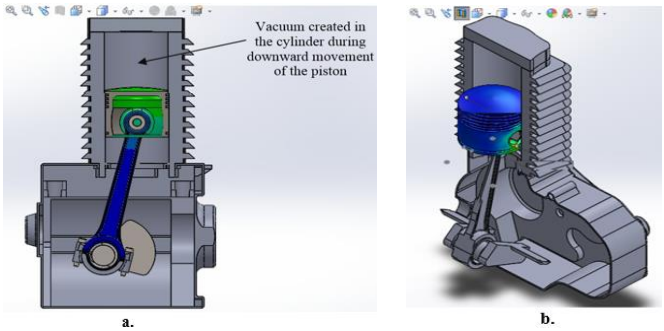

Fig. 9a. Cut section showing downward movement of the piston in IC engine cylinder, 9b. Cut section with piston traveling along the cylinder

The poppet valve gradually closes as the reciprocating piston moves down the cylinder because of increased crankcase pressure development. Before the end of the stroke, the compressed air-fuel mixture in the crankcase expands, as seen in Fig. 10. The enlarged air-fuel combination can then enter the main cylinder and undergo compression and expansion at high temperatures and pressures before being discharged from the IC engine thanks to the intake port being exposed by the reciprocating piston as it approaches the end of its stroke. Particle Image Velocimetry (PIV) in this study were analyzed from the simulated engine geometry CAD profiles. The analyzed PIV were velocity vectors for in-cylinder flow at different Valve Lifts, in-cylinder vorticity magnitudes in at different Valve lifts and in-cylinder TKE distributions at different valve lifts. The well-known Navier-Stokes and nonlinear continuity equations, which completely describe the flow of incompressible, Newtonian fluids, are the partial differential equations regulating fluid flows.

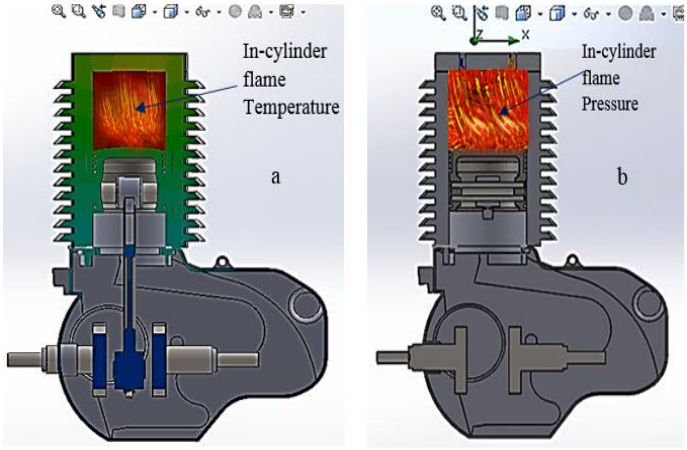

Fig. 10a. Cut section showing in-cylinder flame temperature, 10b. Cut section showing in-cylinder flame pressure

Governing continuity and Navier-Stokes equations are typically used as closed-form non-linear solutions for complex flow problems like the in-cylinder flow in spark ignition engines. These solutions take into account pertinent assumptions, suitable boundary conditions, order of magnitude analysis, and the use of dimensionless parameters. It was assumed that the flow was turbulent, three-dimensional, incompressible, and steady. The analysis is based on a closed cycle with a constant volume of working fluid, but the elements are non-linear and not uniformly spaced. Based on 3D Continuity and Navier Stokes Equations (1, 2, and 3), represented in Cartesian coordinates, the mass and pressure dynamics of the in-cylinder charges at varying valve lift were simulated while applying the boundary conditions.

i. Continuity Equation: A continuity equation defines a conservation law by equating the net flux over the surface with a loss or gain of material within the surface. The continuity equation in this case is represented by Equation 1 as either an integral or a differential equation.

$$\frac{\partial u}{\partial x}+\frac{\partial u}{\partial y}+\frac{\partial u}{\partial z}=0 \tag{1}$$

ii. Energy Equation: This equation demonstrates that the change in energy of the fluid moving through the control volume is equal to the rate of heat transfer into the control volume plus the rates of work done by surface forces plus the rates of work done by gravity as given in Equation 2.

$$\frac{\partial}{\partial t}\left(\rho e+\frac{1}{2}\rho v^2\right)+\frac{\partial}{\partial x}\left(\rho ue+\frac{1}{2}\rho uv^2\right)+\frac{\partial}{\partial y}\left(\rho ve+\frac{1}{2}\rho vv^2\right)+$$

$$\frac{\partial}{\partial z}\left(\rho we+\frac{1}{2}\rho wv^2\right)=k\left(\frac{\partial^2 T}{\partial x^2}+\frac{\partial^2 T}{\partial y^2}+\frac{\partial^2 T}{\partial xz^2}\right)-\left(u\frac{\partial \rho}{\partial x}+v\frac{\partial \rho}{\partial y}+\right.$$

$$w\frac{\partial \rho}{\partial z}\Big)+\mu\left[u\frac{\partial^2 u}{\partial x^2}+\frac{\partial}{\partial x}\left(v\frac{\partial v}{\partial x}+w\frac{\partial w}{\partial x}\right)+v\frac{\partial^2 u}{\partial y^2}+\frac{\partial}{\partial y}\left(u\frac{\partial u}{\partial y}+\right.\right.$$

$$w\frac{\partial w}{\partial y}\Big)+w\frac{\partial^2 u}{\partial z^2}+\frac{\partial}{\partial z}\left(u\frac{\partial u}{\partial z}+v\frac{\partial v}{\partial z}\right)\Big]+2\mu\left[u\frac{\partial^2 u}{\partial x^2}+\frac{\partial u}{dy}\frac{\partial v}{\partial x}+\frac{\partial^2 v}{\partial y^2}+\right.$$

$$\left.\frac{\partial v}{\partial z}\frac{\partial w}{\partial y}+\frac{\partial^2 w}{\partial z^2}+\frac{\partial w}{\partial x}\frac{\partial u}{\partial z}\right]+\rho ug_x+\rho vg_y+\rho wg_z \tag{2}$$

iii. Equations for momentum (Navier Stokes) The momentum equation, which forms the foundation of Newton's Second Law, links the overall force acting on a fluid element to its acceleration or rate of change of momentum. Newton's second law of motion, F = ma, is the foundation for the x, y, and z momentum equations, which are depicted in Equations 3a–c.

$$pu\frac{\partial u}{\partial x}+\rho v\frac{\partial u}{\partial y}+\rho w\frac{\partial u}{\partial z}=\frac{\partial \rho}{\partial x}+\mu\frac{\partial^2 u}{\partial x^2}+\mu\frac{\partial^2 u}{\partial y^2}+\mu\frac{\partial^2 u}{\partial z^2} \tag{3a}$$

$$pu\frac{\partial v}{\partial x}+\rho v\frac{\partial v}{\partial y}+\rho w\frac{\partial v}{\partial z}=\frac{\partial \rho}{\partial y}+\mu\frac{\partial^2 v}{\partial x^2}+\mu\frac{\partial^2 v}{\partial y^2}+\mu\frac{\partial^2 v}{\partial z^2} \tag{3b}$$

$$pu\frac{\partial w}{\partial x}+\rho v\frac{\partial w}{\partial y}+\rho w\frac{\partial w}{\partial z}=\frac{\partial \rho}{\partial z}+\mu\frac{\partial^2 w}{\partial x^2}+\mu\frac{\partial^2 w}{\partial y^2}+\mu\frac{\partial^2 w}{\partial z^2} \tag{3c}$$

The crank angle and the ratio of the piston rod's length to the crank's length can be used to express the cylinder volume. Additionally, Equation 4a-b [41] provides the cylinder volume at any crank angle, and Equation 6 provides the heat transfer per unit area

of the cylinder wall. The cylinder volume can be expressed using the crank angle and the ratio of the piston rod's length to the crank's length. Equation 6 gives the heat transfer per unit area of the cylinder wall, and Equations 4a-b [42] and 6 give the cylinder volume at any crank angle θ.

$$V = V_c + \frac{V_d}{2}\left(1 + \frac{l}{c} - cos\ \theta - \sqrt{\frac{l^2}{c^2} - sin^2\theta}\right) \quad (4a)$$

$$V(\theta) = V_c\left\{1 + \frac{r-1}{2}\left\{1 - cos\theta + \frac{1}{\varepsilon}[1 - (1 - \varepsilon^2 sin^2\theta)^{0.5}]\right\}\right\} \quad (4b)$$

$$\varepsilon = \frac{\text{stroke}}{\text{2 x length of connecting rod}} \quad (5)$$

$$\frac{dQ}{A} = h\left(T_{gas} - T_{wall}\right) + C\left(T_{gas}^4 - T_{wall}^4\right) \quad (6)$$

In this equation, *Vc* is the clearance volume, *Vd* is the displacement volume, *r* is the compression ratio, and ε is the piston stroke. P is the fluid pressure, ρ is the fluid density, t is the tangential velocity, μ is the fluid dynamic viscosity, z is the radial coordinate, u is the fluid velocity, w is the swirl velocity, d*Q*/A is the heat transfer per unit area, and C stands for the Annand closed cycle coefficient. Equation 7 presents the coefficient of discharge (C_d), Equation 8 provides the orifice area between the valve head and seat, and Equation 9 expresses the non-dimensional rig tumble (NT). Equations 10a-e were also used to calculate in-cylinder charges.

$$C_d = \frac{Q}{A_v * V_o} \quad (7)$$

$$A_v = n * \pi * D^2 * \frac{L}{D} * cos\emptyset\ \left(1 + \frac{L}{D} * sin\emptyset.cos\emptyset\right) \quad (8)$$

$$N_T = \frac{8*G}{\dot{m}*V_o*B} \quad (9)$$

$$C_f = \frac{Q}{A_{seat}*V_o} \quad (10a)$$

$$V_o = \sqrt{\frac{2*\Delta P}{\rho}} \quad (10b)$$

$$A_{seat} = \frac{\pi}{4} D^2_{seat} \quad (10c)$$

$$C_s = \sqrt{\frac{2*k}{k-1} R * T_1 * \left[1 - \left(\frac{P_2}{P_1}\right)^{\frac{k-1}{k}}\right]} \quad (10d)$$

$$TKE - \frac{1}{2}\rho V^2_{rms} = \frac{1}{2}\rho(u^2_{rms} + v^2_{rms}) \quad (10e)$$

Where *G* is the torque measured by an impulse meter, B is the diameter of the cylinder bore, L stands for valve lift, n is the number of intake valves per cylinder, is the valve seat angle of 45 degrees, m is the measured mass flow rate, *Q* is the measured volume flow rate, V_o is the velocity head, C_f is the critical flow factor, A_{seat} is the inner seat area, and D_{seat} is the diameter of the intake valve seat. TKE stands for turbulent kinetic energy, u_{rms} and v_{rms} for RMS *x* and *y* velocities, and for air density.

Using the isentropic flow formula, the flow velocity (C_s) is calculated. P_1 represents the air pressure upstream of the valve, P_2 represents the air pressure downstream of the valve, *R* represents the gas constant, and T_1 represents the air temperature upstream of the valve. Equation 11 provides the generalized governing differential equation for heat conduction, and Equation 12 expresses the variation formulation for a conductive barrier [43, 44]

$$K\nabla^2 T + q_E - \rho C\frac{\partial T}{\partial t} = 0 \quad (11)$$

$$\frac{\partial x_k^{(e)}}{\partial\{t\}^{(e)}} = \begin{bmatrix} k_{11} & k_{12} & k_{13} \\ k_{21} & k_{22} & k_{23} \\ k_{31} & k_{32} & k_{33} \end{bmatrix} \begin{Bmatrix} t_i \\ t_j \\ t_k \end{Bmatrix} = [k]^{(e)}\{t\}^{(e)} \quad (12)$$

K stands for thermal conductivity in both radial and axial directions, q_E for heat conduction per unit volume, *p* for material density, *C* for heat capacity, *T* for temperature, t for time, and $[k]^{(e)}$ for stiffness matrix. Equation 13 gives the linear relationship between the contact boundary variation integral of heat transfer and the temperature of the contact surface, whereas Equation 14 gives the governing differential equation for in-cylinder heat convection. Equation 15 [45] presents the variation formulation for the in-cylinder charge convective boundary.

$$\frac{(\partial x_{bcont.})e}{\partial\{t_s\}^e} = \frac{2\pi h_c r_m r_{ij}}{6cos\theta} \begin{bmatrix} 2 - \frac{\varepsilon}{2} & 1 \\ 1 & 2 + \frac{\varepsilon}{2} \end{bmatrix} \cdot \begin{Bmatrix} \{\{t_s\}^e - \{t_s\}^p\}_1 \\ \{\{t_s\}^e - \{t_s\}^p\}_2 \end{Bmatrix} \quad (13)$$

$$-K\left(\frac{\partial_T}{\partial_n}\right) = h(T - T_\infty) \quad (14)$$

$$\delta x_{bconv.} = \int_A^0 -K\ \left(\frac{\partial_T}{\partial_n}\right)\delta T dS =$$

$$\int_A^O h(T -)\ \delta T\ dS,\ \frac{\partial x_{bconv.}}{\partial\{t_s\}} =$$

$$\frac{2\pi h r_m r_{ij}}{6cos\theta} \begin{bmatrix} 2 - \frac{\varepsilon}{2} & 1 \\ 1 & 2 + \frac{\varepsilon}{2} \end{bmatrix} \begin{Bmatrix} t_{si} \\ t_{sj} \end{Bmatrix} - \begin{Bmatrix} (ht_\infty)_1 \\ (ht_\infty)_2 \end{Bmatrix} \quad (15)$$

The two key variables for the turbulence combustion model are the turbulence kinetic energy (k) and turbulence dissipation rate (ε), which may be found in the subsequent transport equations provided by Equations 16 and 17 [46]. Equation 19 provides the energy of the burned and unburned in-cylinder charge, while Equation 20 expresses it in terms of specific heat. Equations 21a–b and 22 allow for the internal energies of the burned and unburned in-cylinder charges to be represented in terms of the average specific

heat, whereas Equation 23 allows for the expression of the mean internal energy of the burned in-cylinder charge in terms of the mean internal temperature.

$$\frac{\partial}{\partial t}(\rho k) + \frac{\partial}{\partial x_i}(\rho k u_i) = \underbrace{\frac{\partial}{\partial x_j}\left[\left(\mu_k + \frac{\mu_t}{\sigma_k}\right)\frac{\partial k}{\partial x_i}\right]}_{Effective\ \ diffusivity} + G_k + G_b - \rho\varepsilon - \gamma_m \quad (16)$$

$$\frac{\partial}{\partial t}(\rho\varepsilon) + \frac{\partial}{\partial x_1}(\rho\varepsilon u_1) = \frac{\partial}{\partial x_j}\left[\left(\mu + \frac{\mu_t}{\sigma_\varepsilon}\right)\frac{\partial \varepsilon}{\partial x_j}\right] + C_{1\varepsilon}\frac{\varepsilon}{K} + (G_K + C_{3\varepsilon} + G_b) - C_{2\varepsilon}\rho\frac{\varepsilon^2}{k} \quad (17)$$

$$\mu_t = \rho C_\mu \frac{k^2}{\varepsilon} \quad (18)$$

$$\bar{u}_i = \Delta\bar{u}_{f_i}{}^{o}(T_o) + \int_{To}^{T} \bar{C}_{vi}(T')dT' \quad (19)$$

$$\bar{C}_{vi} = \frac{\int_{T_1}^{T_2}(a_i + b_i T)dT}{M_i\ (T_2 - T_1)} = \frac{a_i}{M_i} + \frac{b_i}{2M_i}\ (T_1 + T_2) \quad (20)$$

$$\bar{u}_b = a_b + \bar{C}_{vb}\ T_b \quad (21a)$$

$$\bar{u}_u = a_u + \bar{C}_{vu}\ T_u \quad (21b)$$

$$\langle\bar{u}_b\rangle = \int_0^\alpha\ [a_b + \bar{C}_{vb}\ T_b(\alpha, \alpha')]\ d\alpha' \quad (22)$$

$$\langle\bar{u}_b\rangle = a_b + \bar{C}_{vb}\ \langle T_b\rangle \quad (23)$$

Where *YM* stands for the contribution of fluctuation dilation on compressible turbulence to the overall dissipation rate, G_k and G_b stand for the generation of turbulent kinetic energy due to mean velocity gradient of charge, σ_k and σ_ε for the turbulent Prandtl number (Pr) of k and ε, C_μ, $C_{1\varepsilon}$ and $C_{2\varepsilon}$ for constant variables, $(\bar{C}_{vi})$ for the in-cylinder charge specific heat, u and heat coefficient, and mass flow rate is represented by *M*.

Equation 24 gives the force generated by the in-cylinder charge during the compression stroke as the product of the cylinder's maximum pressure and area; Equation 25 gives the torque generated solely by the in-cylinder charge pressure [47].

$$F_g = P_{max}\ \frac{\pi B^2}{4} \quad (24)$$

$$T_g = P_g\ Ar\ sin\theta\ \left[1 + \frac{r}{l}cos\theta\right] \quad (25)$$

During combustion, the in-cylinder adiabatic flame temperature for a lean mixture is given by Equation 26a-c [48], while that of a rich mixture is given by Equation 27 [49].

$$T_R \cong T_o + \frac{m_f.LHV + (m_a + m_f)\bar{C}_{p,R}(T_R - T_o)}{(m_a + m_f)\bar{C}_{p,P}} \quad (26a)$$

$$T_R + \frac{m_f.LHV}{(m_a + m_f)\bar{C}_{p,P}} = T_R + \frac{\frac{m_f}{m_a}LHV}{\left(1 + \frac{m_f}{m_a}\right)\bar{C}_{p,P}} \quad (26b)$$

$$T_R + \frac{f.LHV}{(1+f)\bar{C}_{p,P}} = T_R + \frac{\emptyset.f_S LHV}{(1+\emptyset.f_S)\bar{C}_{p,P}} \quad (26c)$$

$$T_P = T_R + \frac{f.LHV}{(1+f)\bar{C}_{p,P}} = T_R + \frac{f_S.LHV}{(1+\emptyset.f_S)\bar{C}_{p,P}} \quad (27)$$

Where f_S is the stoichiometric fuel/air ratio by mass and T_P is the temperature of the adiabatic flame, *mf* and *ma* are the mass of the fuel and air, respectively, and $\bar{C}_{p,P}$ is an average value of specific heat calculated at the average temperature of the reactants and standard temperature. According to Equation 28, the volumetric efficiency of the engine is determined by the amount of air pulled into the cylinder and taking into account the cylinder volume. Equation 29 estimated function of air mass (m_a) and air density (p_a) yields the actual intake air volume (v_a).

$$\eta_v = \frac{v_a}{v_d} \quad (28)$$

$$v_a = \frac{m_a}{\rho_a} \quad (29)$$

Substituting Equation 29 into Equation 28 gives the volumetric efficiency in Equation 30. Since the intake air mass flow rate is measured on an engine dynamometer rather than air mass, air mass flow rate for formulating volumetric efficiency is given by Equation 31.

$$\eta_v = \frac{m_a}{\rho_a * v_d} \quad (30)$$

$$m_{af} = \frac{m_a * Ne}{nr} \quad (31)$$

Where nr is the number of crankshaft rotations required to complete an engine cycle and Ne is the engine speed (for a four-stroke engine, nr = 2). The relation in Equation 32 can be used to rewrite the intake air mass from Equation 31.

$$m_a = \frac{m_{af} * nr}{Ne} \quad (32)$$

Equation 32 is substituted into Equation 30 to produce Equation 33, which represents the volumetric efficiency. Equation 34 provides the intake air density information.

$$\eta_v = \frac{m_{af} * nr}{\rho_a * v_d * Ne} \quad (33)$$

$$\rho_a = \frac{P_a}{R_a * T_a} \quad (34)$$

Ra stands for the dry air gas constant (286.9 J/*kgk*), while P_a and T_a stand for the intake air pressure, temperature, and, respectively,

Ra. The mechanical efficiency of the engine is determined by the break mean effective pressure (BMEP), which is the difference between the indicated mean effective pressure (IMEP) and friction mean effective pressure (FMEP) as stated by Equation 35.

$$BMEP = IMEP - FMEP \quad (35)$$

In contrast, FMEP stands for the total of the pumping mean effective pressure (PMEP), while Equation (36) expresses the mechanical rubbing mean effective pressure (RMEP) and auxiliary mean effective pressure

$$FMEP = PMEP + RMEP + AMEP \quad (36)$$

Equation 37 in this instance gives the mechanical efficiency of the engine, and Equation 38 is produced by substituting Equation 35 into Equation 37.

$$\eta_m = \frac{BMEP}{IMEP} \quad (37)$$

$$\eta_m = \frac{IMEP-FMEP}{IMEP} = 1 - \frac{FMEP}{IMEP} \quad (38)$$

From Equation 38, it can be seen that the mechanical efficiency increases with decreasing friction losses in a particular IC engine, and the fuel consumption decreases while the power output increases. The lower the FMEP, the higher the mechanical efficiency.

3. Results and Discussion

This section of the study presents the findings from the computation of in-cylinder charge behavior at various valve lift opening clearances in a Renault engine with four-stroke spark ignition and reciprocating internal combustion.

3.1. Temperature of charge in the cylinder at various crank speeds

Losses from molecular dissociation and the fact that there is less energy in the extremely hot combustion gas available for the movement of the piston because it somehow manifests as molecular rotation and vibration are two key drawbacks of high combustion temperatures. This is a key development in the way that running a low mixture cuts down on fuel usage. Leaning the mixture reduces losses from the aforementioned causes, increases fuel efficiency, and lowers the peak combustion temperature [50, 51].
When the engine is in service, the piston is propelled by the hot gas molecules' speed as they come into touch with it and push it. But at high in-cylinder combustion temperatures and pressures, energy in the form of molecular rotations and vibrations which happen more frequently-does not drive the piston; instead, it escapes through the exhaust pipe. Fig. 11-15 shows a graph of the temperature of the cylinder charge for various valve lift opening clearances ranging from 5 to 13 mm at engine speeds between 1000 and 12000 rpm.

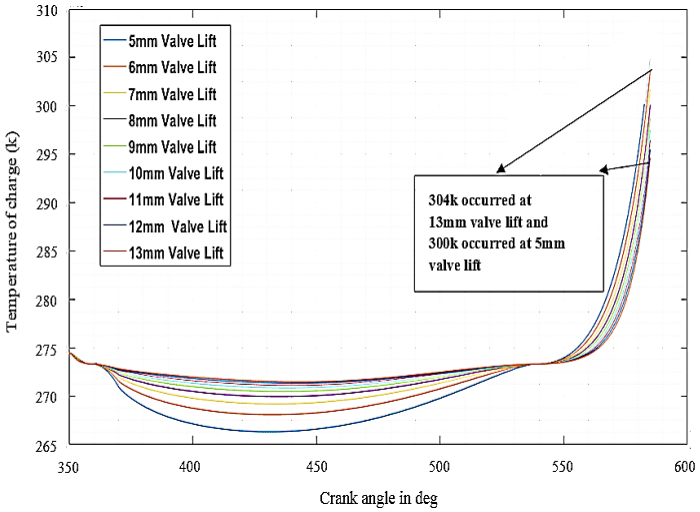

Fig. 11. Temperature of charge in the cylinder @ 1000 rpm for different valve lift at early part of intake stroke

Fig. 11 depicts the relationship between the charge temperature and crank angle during the intake process. A close look at the plot reveals that the temperature of the charge following the intake process rose in correlation with an increase in valve lift at 1000 rpm. This suggests that more valve lift during the intake process at 1000 rpm led to a higher charge temperature. The amount of charge that was swallowed into the cylinder during the intake stroke is what caused this. That is, more charge amount surged through the intake valve opening into the cylinder where it underwent thermal reaction after being ignited and combusted at a high temperature and pressure. This was because the valve lift opening clearance increased.

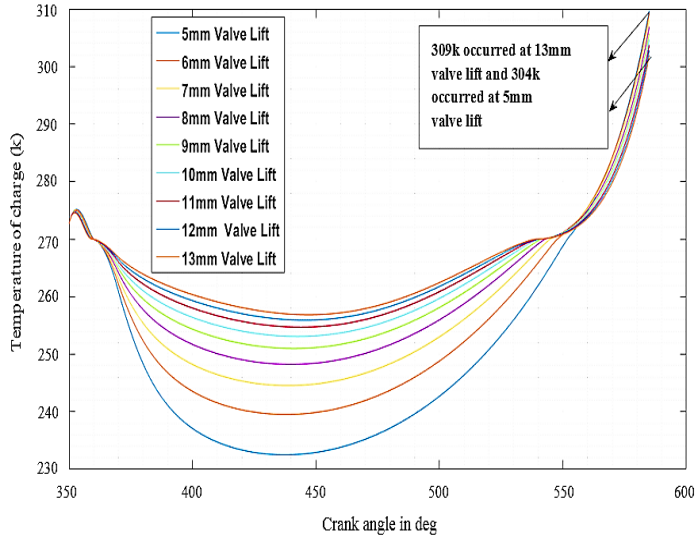

Fig. 12. Charge-in Temperature within the cylinder @ 3000 rpm at early part of intake stroke

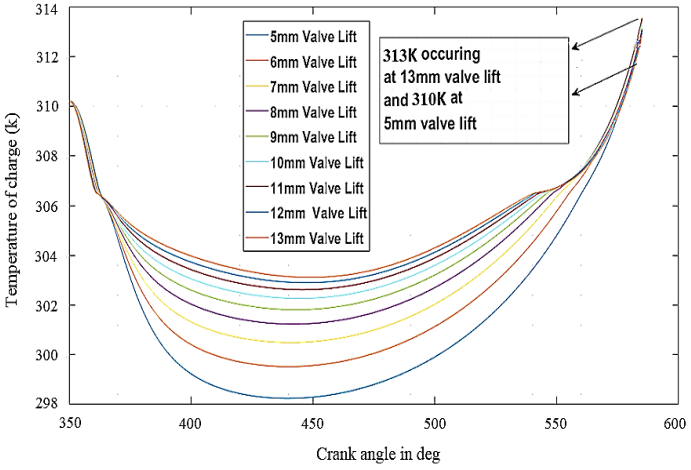

Fig. 13. Charge-in Temperature @ 6000 rpm at early part of intake stroke

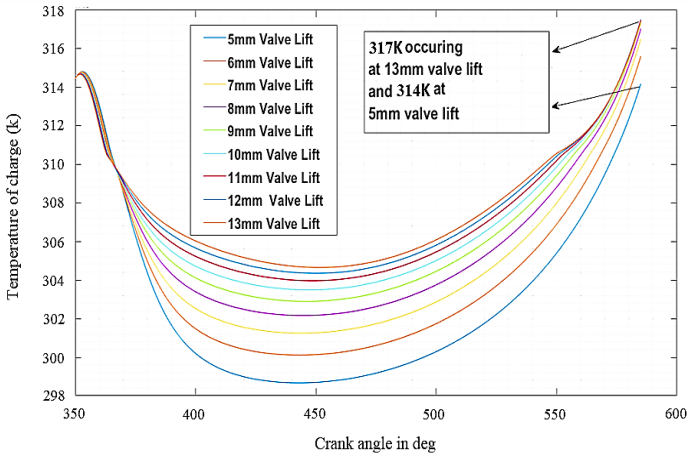

Fig. 14. Charge-in Temperature within the cylinder @ 9000 rpm at early part of intake stroke

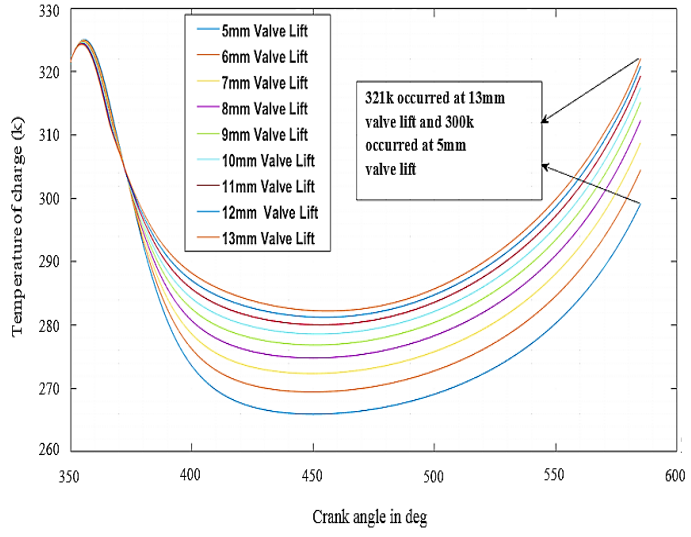

Fig. 15. Charge-in Temperature within the cylinder @ 12000 rpm at early part of intake stroke

Along with an increase in engine speed, the temperature inside the cylinder also rises when the air-fuel ratio rises. Similar to how engine speed and equivalent ratio improve, volumetric efficiency does as well [51]. Variable Valve Timing (VVT) technology is used in four-stroke IC engines to vary the volumetric efficiency in accordance with changes in engine speed. As a result, the valves are uncontrollably opened for a longer amount of time at higher engine speeds to transport the air and charge into and out of the engine. The intake charge density will be reduced and the combustion temperature may increase if the charge temperature is too high. At lower cylinder charge temperatures, starting the engine becomes more challenging and can contribute to an increase in exhaust emission rate [52], whereas this has the potential to limit engine output while also increasing the rate of exhaust emissions [53]. In other words, the release of nitrogen oxides can also result from hotter combustion gases produced by extremely high volumetric efficiency and rising compression.

As indicated in Fig. 11, the temperature of the charge was observed to be 304 K at 13 mm valve lift and 300 K at 5 mm valve lift at engine speeds of 1000 rpm for crank angles ranging from 350 to 600 deg. Because it might raise the charge's total temperature right before combustion, the high cylinder charge temperature is crucial. However, because this engine uses spark ignition, the temperature needs to be watched and managed to prevent auto-ignition before the spark plug creates the spark [54]. The temperature of the charge during the intake process is plotted versus the crank angle in Fig. 12. When the engine was running at 3000 rpm, as opposed to 1000 rpm, the results showed that the temperature of the charge following the intake process increased much more with an increase in valve lifts. As a result, at 3000 rpm and 13mm valve lift for crank angles between 350 and 600 degrees, the temperature of the charge immediately following the intake process was observed to be 309 K, whereas it was 304 K for 5mm valve lift, as shown in Fig. 12. This suggests that increased valve lift at 3000 rpm results in a higher charge temperature following the intake process, just as it does at 1000 rpm engine speed.

The graph of the charge temperature versus crank angle during the intake process is shown in Fig. 13. When compared to the data obtained at engine speed of 3000rpm, further study reveals that the temperature of the charge following the intake process rises further with an increase in valve lift at 6000rpm. This suggests that more valve lift during the intake process at 6000 rpm led to a higher charge temperature. As a result, the temperature of the charge immediately following the intake process is 313 K at 13 mm valve lift while it was 310 K at 5 mm valve lift.

The graph of the charge temperature versus crank angle during the intake process is shown in Fig. 14. When the engine was running at 6000 rpm, the in-cylinder charge temperature was observed to rise from 313 K with a 13 mm valve lift to 317 K with the same valve lift at 9000 rpm. It was also seen to rise from 310 K with a 5 mm valve lift at 6000 rpm to 314 K with the same valve lift at 9000 rpm. The graph of the charge temperature versus crank angle during the intake process is shown in Fig. 15. However, the in-cylinder charge temperature was seen to decrease from 314k with valve lift of 5mm at engine speed of 9000rpm to 300k with the same

valve lift of 5mm at engine speed of 12000rpm. The in-cylinder charge temperature was observed to increase from 317k with valve lift of 13mm at engine speed of 9000rpm to 321k with the same valve lift of 13mm at engine speed of 12000rpm. This might have been brought on by the timing of the valve openings, which, if improperly controlled, might delay the intake and exit of charge from the cylinder. The in-cylinder charge temperature pattern after the intake process was not affected by the incident, as seen by the larger increase in cylinder charge temperature for valves with a 13mm bore at engine speeds of 12000 rpm compared to 9000 rpm.

Maximum valve lift is the highest intake valve opening that provide highest fluid flow to combustion chamber. In the study, valve lift 11, 12 and 13 mm appeared to be very high. The idea for this was to observe the variations and implications they will exhibit compared to valve lifts lower than 11, 12 and 13 mm. It was observed that high valve lift including 11, 12 and 13 mm enabled more air-fuel ratio to enter the combustion chamber, improving the performance of gasoline engine compared to valve lift below these ranges.

Temperature of charge in the cylinder for different valve lifts (see Fig. 11-15) occurred at early part of intake stroke which ranged from 310-330 K. This correlates with the findings of Kurniawan et al. [55] and Fırat and Varol [56], where the wall temperatures at intake stoke is were around 310-320 K, which are 37-47 K higher than the atmospheric temperature.

3.2. Volumetric and Mechanical Efficiency at different Valve Lift and Engine Speed

Thermal efficiency, which defines how well an engine can convert the energy in fuel into heat energy, includes both the mechanical and volumetric efficiencies. These in-cylinder temperature characteristics for the four stroke IC engine were computed using steady-state thermal analysis in the ANSYS Fluent program. In ANSYS fluent, the IGES file format was imported. Then, the penetration parameters for contacted surfaces (Interfaces) between the volumes were established. The inlet pressure in the input valve and the outlet pressure in the output valve were specified as boundary conditions. A dynamic rectangular mesh can be formed in valve motion zones using the layering motion approach and a tetragonal mesh can be created with remeshing while the motion is in motion thanks to the newly created volume. Subsequently all surfaces except the inside of the cylinder had to be chosen for convection. Having done that, the in-cylinder simulation was initiated for mechanical and volumetric efficiencies. Due to the nature of the plots (which were not properly represented, as the x and y axis were not positioned accurately) obtained from ANSYS fluent interface, the plots were represented in Microsoft Excel 2020 edition as shown in Fig. 16-20.

The flow is carried from the intake manifold into the cylinder, where the volumetric efficiency and mechanical efficiency are seen. These two factors are crucial to the engine's performance. This is accomplished via an exhaust port that is situated at the cylinder head. A poppet-style valve is used to open and close the port, and several sets of valves regulate the timing of the flow of exhaust gas into the exhaust port from the cylinder. The ratio of the mass density of the air-fuel mixture pulled into the cylinder at atmospheric pressure during the intake stroke to the mass density of the same volume of air in the intake manifold is known as the volumetric efficiency of an internal combustion engine (IC). The mechanical efficiency is determined by the break power to indicated power ratio (delivered power to the piston versus indicated power).

Although more charge is introduced into the cylinder at higher valve lift, the in-cylinder thermal characteristics of the charge and the pressure during combustion are susceptible to losses at higher valve lift, which can lead to the degradation of the flow stability density functions [27], which may have an impact on the engine's overall performance efficiency. The volumetric efficiency and mechanical efficiency of the engine are plotted against valve lift ranging from 4 to 13 mm and engine speed ranging from 1000 to 12000 rpm, respectively, in Fig. 16-20. It is clear from the plots in Fig. 16-20 that the engine will operate more effectively as a result of the continuous increase in valve lift opening, which has improved engine performance in terms of a comparable increase in volumetric efficiency and mechanical efficiency at all valve lift openings. As the valve lifts and engine speeds increased, both of these engine parameters (volumetric efficiency and mechanical efficiency) indicated a steady increase.

In other words, design of the intake system plays a significant role in determining volumetric efficiency. As engine speed increases, the intake valves open and close more frequently, allowing a greater volume of air-fuel mixture to enter the combustion chamber. This increased intake valve opening duration enhances the engine's ability to draw in a larger amount of air-fuel mixture, thereby improving volumetric efficiency. Valve timing and lift also impact volumetric efficiency. Therefore, at higher engine speeds, the intake valves open earlier and close later, allowing more time for the air-fuel mixture to enter the combustion chamber. The increased valve lift enables a larger volume of air-fuel mixture to be drawn in during each intake stroke. These factors contribute to the continuous increase in volumetric efficiency with rising engine speed. Inertia effects, particularly in the intake system, influence volumetric efficiency. As engine speed increases, the inertia of the air-fuel mixture and the intake air itself becomes more significant. This inertia helps to fill the combustion chamber more effectively, resulting in improved volumetric efficiency. The higher the engine speed, the greater the inertia effects, leading to a continuous increase in volumetric efficiency. Pressure waves and resonance phenomena also contribute to the increase in volumetric efficiency with engine speed. As the engine speed rises, pressure waves generated during the intake stroke can be utilized to enhance the filling of the combustion chamber. These waves create a resonance effect, which aids in drawing in a larger volume of air-fuel mixture. Consequently, volumetric efficiency continues to improve as engine speed increases.

The plot of volumetric and mechanical efficiency was shown to continue its upward trend when the valve lift opening clearance rose, but it was also seen that this upward trend continued as the engine speeds rose. Thus, the higher the thermal efficiency, the better the engine's emissions will be, and the higher the volumetric

efficiency. This is because with higher volumetric efficiency, the rate of mechanical losses is at its peak and more air (more oxygen to support the combustion of air-fuel mixture) is ingested into the cylinder which contributes to higher mechanical efficiency. Therefore, as engine speed increases, the mechanical losses also experiences an increase, leading to increase in mechanical efficiency. Therefore, the relationship between engine speed and mechanical efficiency is complex and multifaceted. As speed increases, mechanical efficiency tends to improve due to reduced frictional losses, decreased internal resistance, the flywheel effect, and optimal operating conditions. Understanding these factors is crucial for designing and operating mechanical systems with enhanced efficiency. Mechanical losses in engines continuously increase as the engine speed rises due to various factors such as frictional losses, aerodynamic losses, increased heat generation, and inefficiencies in lubrication which are highlighted as follows:

i. Friction occurs between various moving parts, such as pistons, crankshafts, and bearings. As engine speed increases, the relative motion between these components intensifies, leading to higher frictional losses. The increased contact area and speed result in greater energy dissipation, causing a rise in mechanical losses
ii. As the engine speed increases, the airflow through the intake and exhaust systems becomes more turbulent, resulting in increased resistance. This increased resistance leads to higher energy losses due to aerodynamic drag, ultimately contributing to the overall mechanical losses.
iii. With higher engine speeds, the combustion process becomes more rapid, generating increased heat. This rise in heat production leads to higher thermal losses, as a significant portion of the energy is dissipated as waste heat. The increased heat generation necessitates additional cooling mechanisms, which further contribute to mechanical losses.
iv. Lubrication is crucial for reducing friction and wear between moving engine components. However, at higher engine speeds, the lubrication system may face challenges in maintaining an adequate oil film thickness and pressure. Inadequate lubrication can result in increased friction and wear, leading to higher mechanical losses.

Any engine can achieve a maximum volumetric efficiency of 1.00, or 100%. With this figure, the engine is able to theoretically draw the maximum volume of fuel and air into the cylinder for combustion. As a result, the volume of the air-fuel intake combination in the engine increases with volumetric efficiency. The shape of the intake manifold, intake air pressure, intake air temperature, intake air mass flow rate, etc., all affect an IC engine's volumetric efficiency. Thus 100% mechanical efficiency is only possible when the engine's output power is equal to its input energy; otherwise, the engine is unable to produce 100% of its potential output. This is caused by a number of things, including friction losses, the forced quick flow of air in the crank case, heat losses, pumping losses at low or cruising throttle, thermal losses to the exhaust and cooling systems, valve and bearing operations, part wear and tear, etc [57]. A given engine cannot produce 100% of its potential power since, while running, it loses some of that power to the wheels they are moving, the clutch, the transmission, the axles, the bearings, etc., which reduces the mechanical efficiency. The ability to increase power by increasing engine speed (rpm) has its limits since friction loss increases as revs climb. In general, an increase in volumetric efficiency enhances an engine's power output. In an engine with more air mass, there is more, and with more fuel, the engine produces more power [58, 59].

Fig. 16 depicts the relationship between volumetric efficiency and mechanical efficiency for an engine running at 1000 rpm with a valve lift clearance of 5 to 13 mm. The graphic displays how, for each engine speed, different valve lift openings affect the volumetric and mechanical efficiency of the engine. When the plot is carefully examined, it becomes clear that at 1000 rpm, the volumetric efficiency and mechanical efficiency improved as the valve lift increased, and vice versa.

It simply means that a higher value of valve lift would increase the volumetric and mechanical efficiency of an engine running at a low engine speed, and a higher value of valve lift would significantly increase the volumetric and mechanical efficiency of an engine running at a high engine speed. At 1000 rpm, the maximum volumetric efficiency for a 5mm valve lift opening clearance was 87.8%, while the maximum volumetric efficiency for a 13mm valve lift opening clearance was 90.7%. At 1000 rpm, a valve lift opening of 5 mm yielded the highest mechanical efficiency of 85.1%, while a valve lift of 13 mm displayed the highest mechanical efficiency of 88.3%, as shown in Fig. 16. The plot shows that as the valve lift opening clearance increased, so did volumetric efficiency and mechanical efficiency.

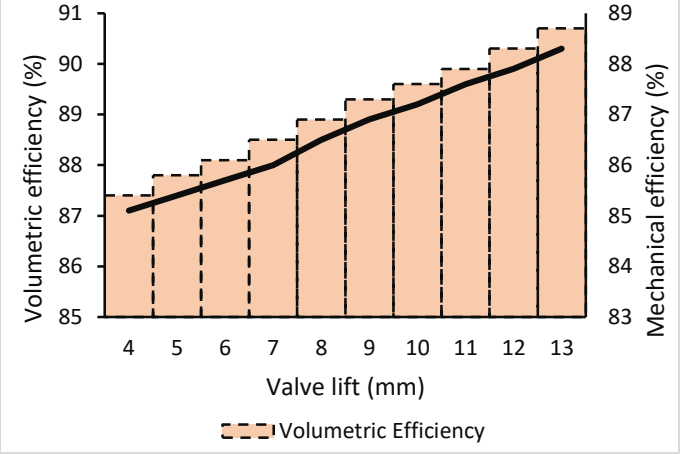

Fig. 16. Efficiency of the engine vs. valve lift @1000 rpm

A plot of volumetric and mechanical efficiency vs. valve lift at 3000 rpm is shown in Fig. 17. The maximum volumetric efficiency for 5mm valve lift opening clearance at 3000 rpm was 90.9%, while the maximum volumetric efficiency for 13mm valve lift was 93.7%. For 3000 rpm, maximum mechanical efficiency was also attained for valve lifts of 5mm and 13mm, respectively, yielding 88.2% and 91%, respectively, of mechanical efficiency. The plot shows that as the valve lift opening clearance also increased, both volumetric efficiency and mechanical efficiency increased.

Additionally, it was found that for all valve lift opening clearances, the volumetric and mechanical efficiencies attained at a high engine speed (3000 rpm) compared to the prior (1000 rpm) were similarly higher.

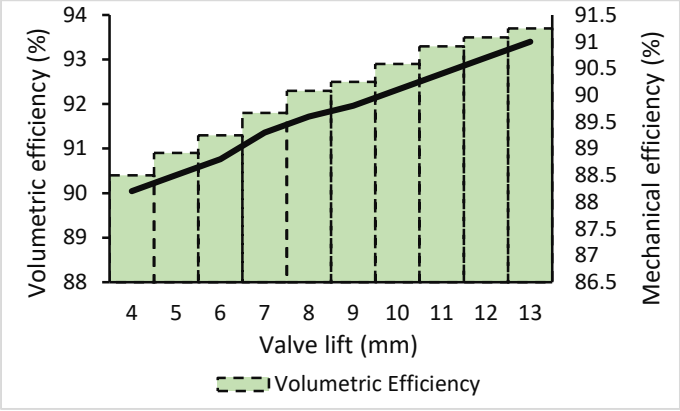

Fig. 17. Efficiency of the engine vs. valve lift @ 3000 rpm

Fig. 18 displays the relationship between volumetric and mechanical efficiency and valve lift clearance ranging from 5 to 13 mm at 6000 rpm. At 6000 rpm, a 5mm valve lift demonstrated a maximum volumetric efficiency of 92.4%, while a 13mm valve lift opening clearance showed a maximum volumetric efficiency of 95.7%. A valve lift opening clearance of 5mm demonstrated a maximum mechanical efficiency of 91.2% at 6000 rpm, while a valve lift opening of 13mm showed a mechanical efficiency of 94%. Additionally, it was found that for all valve lift opening clearances, the volumetric and mechanical efficiencies attained at a high engine speed (6000 rpm) compared to the prior (3000 rpm) were similarly higher.

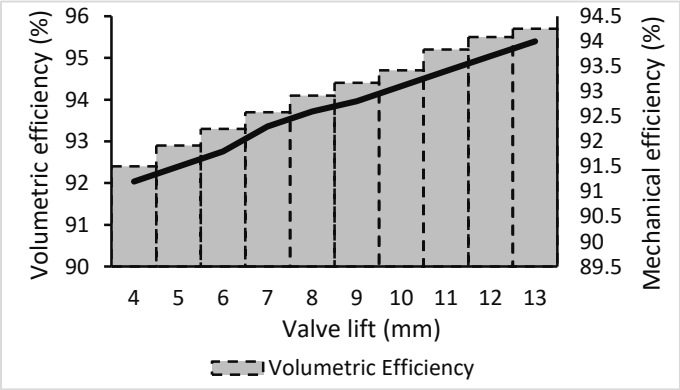

Fig. 18. Efficiency of the engine vs. valve lift @ 6000 rpm

Fig. 19 depicts the relationship between volumetric and mechanical efficiency and valve lift clearance, which ranges from 5 to 13 millimeters at 9000 rpm. At 9000 rpm, a valve lift opening clearance of 5 mm produced volumetric efficiency of 94.2%, while a valve lift opening of 13 mm produced volumetric efficiency of 97.7%. Additionally, at 9000 rpm, the mechanical efficiency of the 13mm valve lift opening was 95.7%, compared to the highest mechanical efficiency of 93.3% for the 5mm valve lift opening. Additionally, it was found that all valve lift opening clearances had higher volumetric and mechanical efficiencies at high engine speeds (9000 rpm) than at lower engine speeds (6000 rpm).

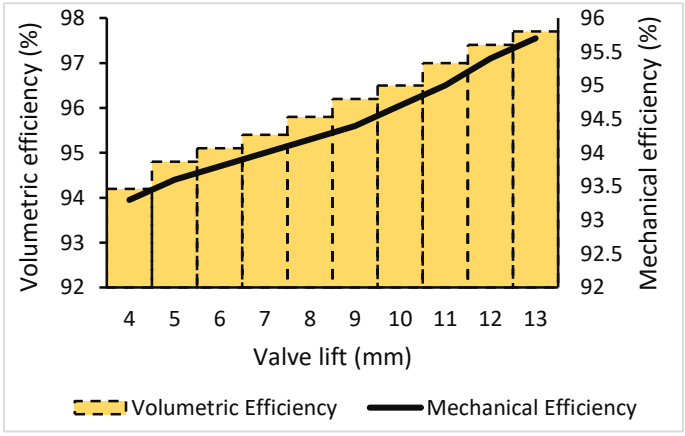

Fig. 19. Efficiency of the engine vs. valve lift @ 9000rpm

Fig. 20 displays the relationship between volumetric and mechanical efficiency and valve lift clearance, which ranges from 5 to 13 mm at 12000 rpm. At 12000 rpm, a 5mm valve lift opening clearance exhibited a maximum volumetric efficiency of 95.2%, while a valve lift opening clearance of the same size yielded a volumetric efficiency of 98.7%. Additionally, at 12000 rpm, the mechanical efficiency of the 5mm and 13mm valve lift openings was 95.4% and 97.8%, respectively, for the 5mm valve lift opening. Additionally, it was found that all valve lift opening clearances had higher volumetric and mechanical efficiency at a high engine speed (12000 rpm) than at a lower engine speed (9000 rpm).

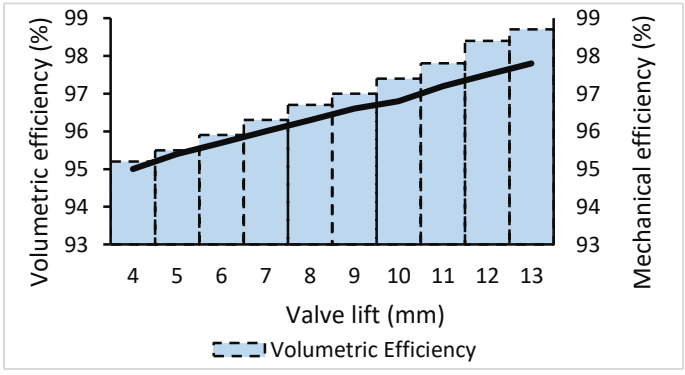

Fig. 20. Efficiency of the engine vs. valve lift @ 12000rpm

3.3. Velocity vectors for in-cylinder flow at different Valve Lifts

Both high and low flow velocity regimes define in-cylinder flow fields. By use of a directed intake manifold and a moving piston, spark ignition (SI) engines are particularly prone to tumble motion, which produces a substantial tumble vortex in areas with low flow

velocities surrounding the vortex centres [60]. The discrepancies between vector fields are produced on a spatially resolved map by metrics like the relevance index (RI). However, due to a greater relative shift in the alignment of the vectors close to the vortex centres, a little difference in in-cylinder velocity may have a substantial impact on RI along the regions with low in-cylinder velocity.

The spatially averaged RI of a pair of flow fields is dominated by minute absolute differences in velocity that cover other differences that may exist in high velocity regions of the flow close to the centre of the tumble vortex, where velocity magnitudes are low and flow direction varies significantly over short distances (reversing across the centre of the vortex) [61]. Fig. 21 depicts the ensemble PIV average velocity vector fields in a reciprocating spark-ignition IC engine with valve lift opening clearances of 5, 7, 10, and 13 mm with a speed of 9000 rpm.

The colour red at the top of the colour band represents the maximum values, while the colour royal blue at the bottom of the colour band represents the minimum values. The three components that make up the velocity vector field, diagonal vector (v), horizontal vector (v_x), and vertical vector (v_y), all indicate how the in-cylinder charge behaves or flows when the engine is operating in service condition. It was found that there was a significant concentration of air-fuel combination coming through the intake valve at a valve lift of 13 mm, and this was apparent at the centre of the cylinder. The colour band at the bottom of PIV in Fig. 21 represents the strength of velocity vector fields and ranges from 0-0.8 m/s.

The colour yellow on the colour wheel denotes the highest value, whereas the colours lemon, light blue, and royal blue denote the lowest value. The symmetric velocity distribution along the intake valve and exhaust valve, as shown by the velocity vector fields at 13 mm valve lift, resulted in considerable flow rotation and distributions with swirl and tumble motion. Additionally, the high concentration of horizontal, parallel, and yellow lines in the velocity flow fields showed that the engine is ingesting a significant amount of air-fuel mixture when the intake valve opens at 13 mm, raising the temperature and pressure of the combustion flame.

As opposed to the case stated for intake valve lift opening clearance of 13 mm, this is different for intake valve lift opening of 10 mm, which experienced reduction in the cylinder. As a result, with a valve lift opening clearance of 10 mm, the concentration of the air-fuel mixture entering the intake valve started to decrease while spreading outward to the cylinder walls, whereas in the case of a valve lift opening clearance of 13 mm, the flow pattern appeared to converge. As a result of in-cylinder reductions in the supply rate of air-fuel mixture and reductions in the valve lift opening clearance, further reductions were observed in the velocity vector fields at intake valve lift of 7 mm than had been reported for intake valve lift of 10 and 13 mm.

As a result of in-cylinder reductions in the supply rate of air-fuel mixture and reductions in the valve lift opening clearance, more reductions in the velocity vector fields were observed at 5 mm intake valve lift opening clearance than had been reported for cases at 7, 10, and 13 mm. From Fig. 21, it is clear that as the valve lift decreases, so too do the velocity vectors for in-cylinder flow in the IC engine model examined in this study. This happens as the valve orifice gets smaller, which slows the rate at which fuel and air are injected into the cylinder. For intake flow, a velocity vector range of 20-30 m/s is often considered optimal. This range ensures sufficient air-fuel mixing while minimizing pressure losses. Higher velocities may lead to increased pressure drops and reduced volumetric efficiency, while lower velocities may result in inadequate mixing and reduced combustion efficiency. In the combustion chamber, a velocity vector range of 30-40 m/s is commonly recommended. This range promotes efficient fuel-air mixing and combustion stability. Higher velocities may cause excessive turbulence and increased heat losses, while lower velocities may result in incomplete combustion and increased emissions. By considering factors such as fuel-air mixing, heat losses, and combustion stability, specific ranges for the velocity vector can be determined. The recommended ranges of 20-30 m/s for intake flow and 30-40 m/s for the combustion chamber provide a starting point for achieving optimal engine performance. However, it is important to note that these values may vary depending on the engine design and operating conditions.

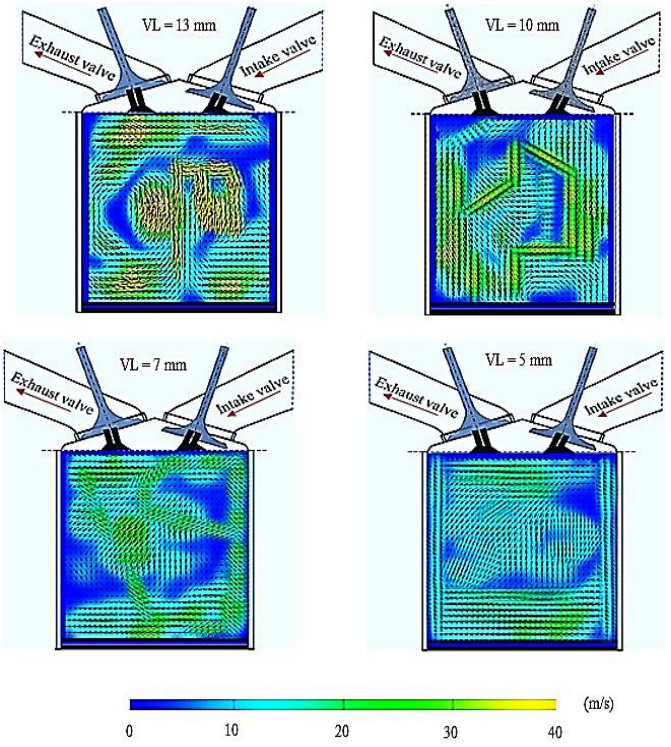

Fig. 21. PIV showing velocity vector fields at various valve lifts

3.4. In-cylinder Vorticity Magnitudes in at different Valve Lifts

The PIV vorticity magnitudes at various valve lifts are shown in Fig. 22. The flow patterns are shown rotating in a counter clockwise manner in the green sections and a clockwise direction in the blue parts. As can be observed, clockwise vortices formed behind the intake valves at lower valve lifts (5 mm), which led to an increase in vorticity strength as the valve lift increased.

From the PIV in Fig. 22, it is clear that an increase in valve lift increased flow speed while simultaneously varying flow patterns, resulting in a counter clockwise vortex motion (tumble). At a valve lift of 5 mm on the right side of the cylinder, the tumble motion first appeared. At a valve lift of 7 mm, it became stronger and moved toward the centre, then the upper half of the cylinder. The vortices had become more intense at 10 mm of valve lift because of the increased cylinder flow speed at high temperature and pressure. The agitating vortices in the cylinder were fully saturated at valve lift 13 mm, and the predominant component of the air-fuel mixture at this time was hot gases. The valve lift at 13 mm is wide open, which causes the flow of the air-fuel combination into and out of the cylinder to intensify with high levels of combustion.

At this point, full combustion occurs with a low degree of emissions if the appropriate amount of fuel is injected together with the air inhaled. According to Krishna and Mallikarjuna [62], the interaction of the air-fuel mixture with the cylinder walls and the surface of the piston, as well as the narrow passage of the intake valves and cylinder, are likely to lead to the formation of vortices and random flow of hot in-cylinder charges. Due to the form of the piston, the orientation of the intake manifold, the lift of the intake valve, and the engine speed, in-cylinder flows in an IC engine can be divided into parallel (swirl) and perpendicular (tumble) flows during the intake, compression, and expansion strokes [63].

The flow movement happens within the cylinder from the right to the left side, guided by the top surface of the reciprocating piston and the cylinder walls, resulting in the formation of vortices with various patterns. According to a related study by Heywood [64], creating a sizable vortex flow (swirl and tumble) inside an IC engine cylinder during the intake process causes large levels of turbulence to occur later in the compression stroke, which causes rapid burning rates. In the premixed SI engines, Hill and Zhang [65] found that vortex flows could greatly increase the turbulence during the combustion phase, resulting in a shorter burning time and higher thermal efficiency. Several experimental studies have investigated the effects of vorticity on engine performance. These studies have shown that an optimally accepted range of vorticity values exists, typically between 150 and 210 s^-1 as represented by lemon colour on the legend in Fig. 22. Within this range, the combustion process is enhanced, resulting in an improved air-fuel mixing, reduced emissions, improved flame propagation and combustion stability as well as increased thermal efficiency. This correlate with the findings of El-Adawy et al. [17] who experimentally investigated IC engine in-cylinder flow using different steady-state flow benches. However, excessive vorticity can lead to increased turbulence levels, which may result in incomplete combustion, higher emissions, and reduced engine efficiency. The efficiency and performance of these engines depend on several factors, including the flow characteristics within the combustion chamber. Therefore, determining the optimal range of vorticity values is crucial for achieving efficient combustion. 3.5. In-cylinder TKE Distributions at different Valve Lifts.

Air-fuel mixture enters the engine's cylinder on the right side as a jet, which travels parallel to the cylinder head before turning downward upon hitting the cylinder's top. It strikes the piston crown's top surface once more, creating a clockwise vortex.

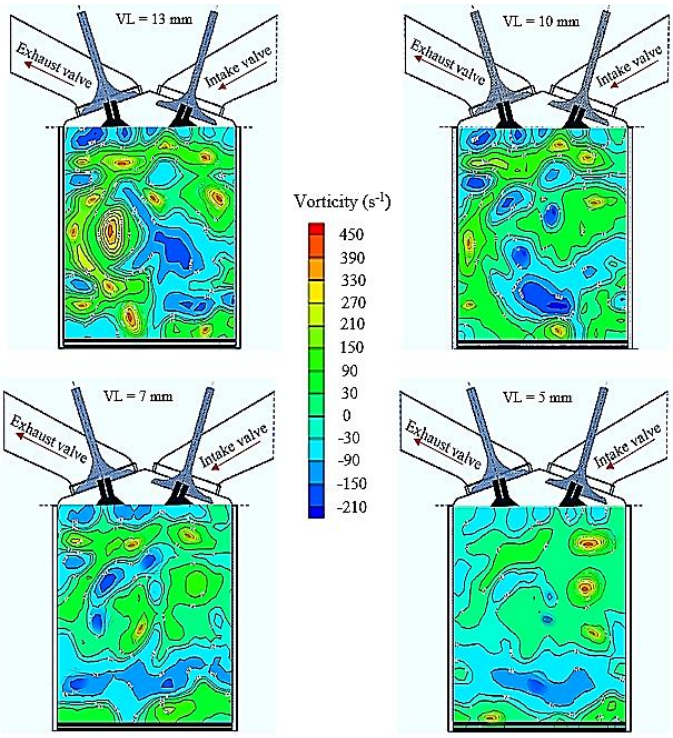

Fig. 22. PIV showing vorticity magnitudes at different valve lifts

Similar to this, a little amount of air-fuel mixture that enters the cylinder by the intake valve's left side strikes the cylinder's left side, diverting downward, and then impacts the piston's top surface again, diverting upward and creating a counter clockwise vortex.

Particle Image velocimetry showing the TKE in-cylinder flow patterns at various valve lift opening clearances are shown in Fig. 23. Whether or not the TKE is severe is indicated by the colour band in the middle of the plots. The colour band shows that red has the highest TKE, followed by orange, yellow, lemon, light green, sky blue, and royal blue. Yellow, lemon, light green, sky blue, and royal blue have the lowest TKE. The values assigned to each colour on the colour band determine this situation .Due to the presence of red and yellow traces on the TKE profile, it can be seen that TKE at valve lift openings of 13 mm appears to be the highest. On the TKE profile, it was found that the appearance of these colours decreased at 10 mm of valve lift. As the valve lift opening shrunk, additional decreases (in valve lift 7 and 5 mm) in these colours were seen.

The spirally rotating patterns that denote turbulent flows also appeared to be more intense and complex at higher valve lift opening clearances, such as 13 mm, due to an increase in fluid motion marked by chaotic changes in pressure and flow velocity of the in-cylinder air-fuel mixture, as opposed to lower valve lift opening clearances, such as 5 mm, due to a decrease in the in-cylinder charge's fluid motion. High TKE is important for IC engine cylinder cycles because it improves air-fuel mixing and mixture uniformity, raises charge combustibility, and may even have a leaning

impact [66]. The ratio of kinetic energy to the rate of viscous damping in the flow of the in-cylinder air-fuel mixture can be used to anticipate when turbulence will start to occur in an internal combustion engine cycle [67].

As shown in Fig. 23, the PIV illustrates the TKE in-cylinder flow distributions in three dimensions with unstable vortices and turbulence brought on by the cylinder charge's high kinetic energy. Laminar flow, on the other hand, is when a fluid flows in parallel layers without any interruption between the layers. The low viscosity of the air-fuel mixture from intake stroke through compression and expansion to exhaust stroke was shown to be the main factor in all of the valve lift opening clearance given in this study, as illustrated in Fig. 23.

High diffusivity is another characteristic of turbulent flows in IC engine cylinders, which increases the transfer of momentum, heat, and energy. For instance, turbulent heat transfer in the cylinder happens in a matter of seconds as opposed to hours, and turbulent flames spread more quickly than laminar flames. One distinguishing characteristic of a turbulent flow is that laminar flow instability causes it to develop at high Reynolds numbers.

These instabilities are the result of the interaction of strongly nonlinear viscous and inertial forces. They have dispersed vorticity areas that go through vortex stretching to maintain or grow the quantity of vorticity. Without this ability of the vortex to extend, the kinetic energy in the turbulent flow would quickly deplete. This suggests that turbulent flows are very dissipative, therefore without a steady supply of sufficient amounts of air-fuel combination in the cylinder to maintain the loss to viscosity, the turbulence will decay quickly [68].

Turbulence enhances fuel-air mixing, leading to better in-cylinder combustion efficiency in IC engines. Optimum TKE level affects the degree of mixing, thereby, ensuring a more uniform distribution of the mixture within the combustion chamber, improved flame propagation and reduced flame quenching. This leads to faster and more complete combustion, resulting in improved thermal efficiency and engine performance. Turbulence affects pollutant formation and emissions in IC engines. Higher TKE levels can lead to increased mixing and reduced pollutant emissions. However, excessively high TKE values may result in increased NOx emissions and increased heat transfer to the cylinder walls, reducing the overall combustion efficiency.

Based on the findings available in literature, the optimal range of TKE values in IC engines is found to be between 25 and 40 m2/s2, which in this study is represented by lemon colour on the legend in Fig. 23. Within this range, the fuel-air mixing is enhanced, combustion efficiency is improved, and pollutant emissions are minimized. Variation of TKE obtained at various valve lifts in this study correlates with the findings of El-Adawy et al. [69] who employed stereoscopic particle image velocimetry measurements and orthogonal decomposition to investigate in-cylinder flow of gasoline direct injection engine.

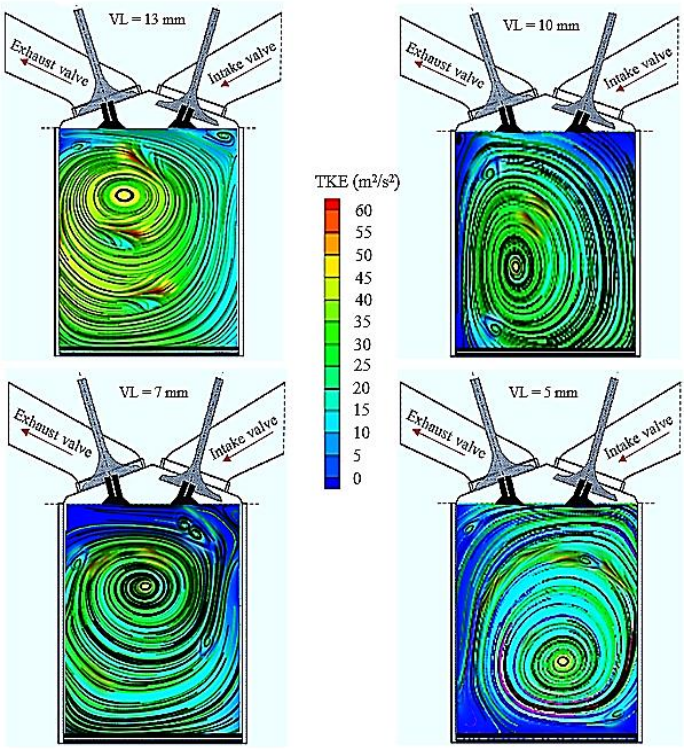

Fig. 23. PIV showing in-cylinder flow distributions of TKE in IC engine

4. Conclusions

The computation of mechanical efficiency in IC engines using ANSYS Fluent software offers a powerful and efficient approach for evaluating engine performance. By accurately simulating the complex flow and combustion processes, ANSYS Fluent enables engineers to optimize engine design and improve fuel efficiency. However, it is crucial to validate and verify the simulation results using experimental data to ensure their accuracy and reliability. In this study, the flow dynamics of a spark-ignition reciprocating internal combustion engine with a four-stroke in-cylinder charge behavior were estimated at different valve lift opening clearances. The following conclusions were drawn from the various computations:

i. Strong in-cylinder tumble motion with high non-dimensional rig-tumble and turbulent kinetic energy distributions generated with greater valve lifts between 10 and 13 mm.
ii. At higher valve lift between 10 and 13 mm, increasing in-cylinder vortex flow (swirl and tumble) took place. This resulted in considerable vorticity magnitudes, which were in turn responsible for higher turbulence during the later phases of the compression and expansion strokes, resulting in rapid burning rates.
iii. It was found that the in-cylinder flow velocity greatly increased between 10 and 13 mm of valve lift and swiftly decreased as the valve lift opening clearance decreased.
iv. During the power stroke, complete combustion was ensured due to the high level of turbulence that was present during the combustion.

v. Time duration of combustion was shortened due to an increase in turbulent flow, which also hastened burning, increased thermal efficiency, and reduced the rate of cyclic changes.
vi. It was found that increasing the cylinder temperature during combustion improved the thermal characteristics of the air-fuel combination while simultaneously having an impact on the thermal cycle at increased valve lift due to heat loss. Although the study did not examine the emission characteristics, this would typically result in a decrease in the emission of hazardous chemicals and an increase in cycle efficiency.

At engine speed of 1000, 3000, 6000, 9000 and 12000 rpm, in-cylinder temperature of charge at 13 mm valve lift were 304, 309, 313, 317 and 321 k while in-cylinder temperature of charge at 5 mm valve lift were 300, 304, 310, 314 and 300 k. At 12000 rpm, the in-cylinder charge temperature was observed to reduce for 5mm valve lift. This is because at this stage, the engine stroke returns to the intake position were fresh air and fuel are drawn into the combustion chamber.

Internal Combustion (IC) engines have revolutionized the transportation industry, powering various vehicles and machinery. As the automotive industry continues to evolve towards more sustainable and efficient technologies, the significance of valve lift in IC engines cannot be overstated. Among the crucial components of an IC engine, the valve lift plays a significant role in determining engine performance and efficiency. Therefore, the present study has contributed to future research in the following ways:

i. A higher valve lift allows for increased airflow, resulting in improved volumetric efficiency and enhanced power output. This increased power output is particularly beneficial in high-performance engines, where maximizing power is a priority.
ii. By controlling the amount of air-fuel mixture entering the combustion chamber, valve lift directly influences the fuel-air ratio. A well-optimized valve lift ensures an appropriate mixture, leading to efficient combustion and reduced fuel consumption. This is especially important in today's environmentally conscious world, where reducing fuel consumption is a key objective.
iii. By regulating the air-fuel mixture, valve lift influences the combustion process, affecting the formation of harmful pollutants such as nitrogen oxides (NOx) and particulate matter (PM). Proper valve lift adjustment can help achieve optimal combustion, minimizing emissions and meeting stringent environmental regulations. Consequently, valve lift control is crucial for reducing the environmental footprint of IC engines.
iv. Valve lift directly affects the engine's overall performance. It determines the engine's ability to breathe efficiently, impacting torque characteristics, throttle response, and overall drivability. A well-designed valve lift profile can enhance low-end torque, providing better acceleration and responsiveness. This is particularly important in applications such as passenger vehicles, where smooth and responsive engine performance is desired.

Hence, by optimizing valve lift, engineers can achieve improved power output, reduced fuel consumption, lower emissions, and enhanced engine performance

List all abbreviations

TKE	: turbulence kinetic energy
RNG k-ε	: turbulence model
SI	: spark ignition
CFD	: computational fluid dynamics
FGM	: flamelet generated Manifold
LES	: large eddy simulation
TFF	: turbulent fluid flow
PIV	: particle image velocimetry
MRV	: magnetic resonance velocimetry
TLS	: turbulent length scale
TDC	: top dead center
BDC	: bottom dead center
RANS	: Reynolds-averaged navier-stokes
RMEP	: rubbing mean effective pressure
RMS	: root-mean-square
VVT	: variable valve timing
V_d	: displacement volume
r	: compression ratio
ε	: piston stroke
P	: fluid pressure
ρ	: fluid density
∂_t	tangential velocity
μ	: dynamic viscosity
z	: radial coordinate
u	: fluid velocity
w	: swirl velocity
dQ/A	: heat transfer per unit area
C	: closed cycle coefficient
C_d	: coefficient of discharge
Q	: mass flow rate
V_o	: volume flow rate
C_f	: critical flow factor
A_{seat}	: inner seat area
D_{seat}	: intake valve seat diameter
u_{rms}	: velocity components
R	: gas constant
Pr	: turbulent prandtl number
G_k and G_b	: turbulent kinetic energy
T_b	: temperature of burned charge
T_u	: temperature of unburned charge
mf	: mass of fuel
ma	: mass of air
$\bar{C}_{p,P}$	: specific heat
T_P	: adiabatic flame temperature
v_a	: intake air volume
m_a	: air mass
p_a	: density of air
v_x	: horizontal vector
v_y	: vertical vector

Conflict of Interest Statement

They authors declare that they had no agreement or financial involvement with anyone, organization or institution in the course of this research work. Therefore, there is no conflict of interest associated with any part of this paper or the publication of this manuscript.

CRediT Author Statement

Aniekan Ikpe: Conceptualization, Content development, Supervision, Review and Editing.
Michael Bassey: Modelling, Simulation, Data curation, Formal analysis and Validation.

References

[1] Kunt MA. Analysis of Engine and Powertrain Losses of a Passenger Type 4-Stroke Gasoline Vehicle in 4 Different Driving Cycles with GT-SUITE Vehicle Simulation Program. Int. J. Automot. Sci. Technol. 2022;6(4):340-346.

[2] Furuhata T, Tanno S, Miura T, Ikeda Y, Nakajima T. Performance of numerical spray combustion simulation. Eng. Convers. Manag. 1997;38(10-13):1111-22.

[3] Godino JAV, Garcia MT, Jimenez-Espadafor Aguilar FJ, Trujillo EC. Numerical study of HCCI combustion fueled with diesel oil using a multizone model approach. Eng. Convers. Manag. 2015;89:885-95.

[4] Owunna IB, Ikpe AE. Comparative Analysis of Four Stroke and Six Stroke Internal Combustion Renault Engine Efficiency Using Matlab Simulation Tool. Nig. J. Eng. 2021;28(3):62-69.

[5] Nagareddy S, Kumar A, Sharma AR, Kumar A. Heat Transfer Correlations on Combustion Chamber Surface of Diesel Engine-Experimental Method. Int. J. Automot. Sci. Technol. 2018;2(3):28-35.

[6] Towoju OA. Performance Optimization of Compresion Ignition Engines. Eng. Persp. 2022;2(2):21-27.

[7] Arslan TA, Kocakulak T. A Comprehensive Review on Sirling Engines. Eng. Persp. 2023;3(3):42-56.

[8] Kurniawan WH, Abdullah S, Shamsudeen A. A computational fluid dynamics study of cold-flow analysis for mixture preparation in a motored four-stroke direct injection engine. J Appl. Sci. 2007;7(19):2710-2724.

[9] Xia B, Sun DW. Applications of computational fluid dynamics (CFD) in the food industry: a review. Comput. Elect. Agric. 2002;34(1-2):5-24.

[10] Guojiang W, Song T. CFD simulation of the effect of upstream flow distribution on the light-off performance of a catalytic converter. Eng. Conv. Manag. 2005;46(13-14):2010-2031.

[11] Semlitsch B, Wang Y, Mihaescu M. Flow effects due to valve and piston motion in an internal combustion engine exhaust port. Eng. Convers. Manag. 2015;96: 18-30.

[12] Bianchi GM, Cazzoli G, Forte C, Costa M, Oliva M. Development of a emission compliant, high efficiency, two-valve DI diesel engine for off-road application. Eng. Proc. 2014;45:1007-1016.

[13] Baratta M, Misul D, Spessa E, Viglione L, Carpegna G, Perna F. Experimental and numerical approaches for the quantification of tumble intensity in high-performance SI engines. Eng. Convers. Manage. 2017;138: 435-451.

[14] Reuss DL. Cyclic variability of large-scale turbulent structures in directed and undirected IC engine flows. SAE Technical Paper, No. 2000-01-0246, 2000.

[15] Voisine M, Thomas L, Bore´ e J, Rey P. Spatio-temporal structure and cycle to cycle variations of an in-cylinder tumbling flow, Exp. Fluids 2011;50(5):1393-1407.

[16] Druault P, Guibert P, Alizon F. Use of proper orthogonal decomposition for time interpolation from PIV data, Exp. Fluids 2005;39(6):1009-1023.

[17] El-Adawy M, Heikal MR, Aziz AR, Siddiqui MI, Hasanain A, Wahhab A. Experimental study on an IC engine in-cylinder flow using different steady-state flow benches. Alex. Eng. J. 2017;56: 727-736.

[18] Nishad K, Ries F, Li Y, Sadiki A. Numerical Investigation of Flow through a Valve during Charge Intake in a DISI -Engine Using Large Eddy Simulation. Eng. 2019;12(2620):1-20.

[19] Kazmouz SJ, Scarcelli R, Cheng Z, Dai M. Pomraning, E., Senecal, P. K. and Sjöberg, M. Coupling a Lagrangian–Eulerian Spark-Ignition (LESI) model with LES combustion models for engine simulations. Sci. Tech. Eng. Trans. 2022;77(10):1-14.

[20] Rahiman A, Razak AR, Samee MA. CFD Analysis of Flow Field Development in a Direct Injection Diesel Engine with Different Manifolds. Ame. J. Fluid Dyn. 2014;4:102-113.

[21] Mohammed E, Heikal MR, Aziz AR, Siddiqui MI, Munir S, Characterization of the Inlet Port Flow under Steady-State Conditions Using PIV and POD. Energies 2017;10(1950):2-16.

[22] Azad AK, Rasul MG, Khan MMK, Sharma SC, Hazrat MA. Prospect of biofuels as an alternative transport fuel in Australia. Renw. and Sus. Eng. Rev. 2015;43:331-351.

[23] Ikpe AE, Owunna IB, John PO. Port Flow Simulation and In-cylinder Swirl Motion Characteristic Effects in Internal Combustion Engine Duty Cycle. Appl. Modl. Sim. 2021;5:102-114.

[24] Kent JC, Haghgooie M, Mikulec A, Davis GC, Tabaczynski RJ. (1987) Effects of Intake Port Design and Valve Lift on In-cylinder Flow and Burnrate. Fuels and Lubr. 1987;97(7):975-987.

[25] Krishna BM, Bijucherian A, Mallikarjuna JM. (2010) Effect of intake manifold inclination on intake valve flow characteristics of a single cylinder engine using particle image velocimetry. Wld. Acad. Sci. Eng. Tech. 2010;68:176-182.

[26] Kapitza L, Imberdis O, Bensler HP, Willand J, The´venin D. An experimental analysis of the turbulent structures generated by the intake port of a DISI-engine. Exp. Fluids. 2010;48:265-280.

[27] Rabault J, Vernet JA, Lindgren B, Alfredsson PH. (2016) A study using PIV of the intake flow in a diesel engine cylinder. Int. J. Ht. Fluid F. 2016;62:56-67.

[28] Wahono B, Setiawan A, Lim O. Experimental study and numerical simulation on in-cylinder flow of small motorcycle engine. Appl. Eng. 2019;255:113863.

[29] Setiadi H, Jones KO, Nugroho TA, Abdillah M, Trilaksana H, Amrillah T. Designof spark ignition engine speed control using bat algorithm. Int. J. Elect. Comp. Eng. 2021;11(1):794-801.

[30] Ikpe AE, Owunna IB. Simulation of Mass and Pressure Dynamics

of In-cylinder Charges at Variable Valve Lift Clearance in Four Stroke Spark Ignition Engine. Adv. Eng. Des. Tech. 2021;3:115-131.

[31] Ikpe AE, Ekanem KR, Etuk EM. Simulation of Internal Pipe Flows In Gasoline Port Fuel Injection System Under Steady State Condition. Usak Uni. J. Eng. Sci. 2021;4(2):79-93.

[32] Mamala J, Tomczuk B, Waindok A, Graba M, Hennek K. Improving the Efficiency of Spark-Ignition Internal Combustion Engine Using a Novel Electromagnetic Actuator and Adapting Increased Compression. Eng. 2023;16,1-17.

[33] Serranno JR, Arnau FJ, Martin J, Aunon A.Development of a Variable Valve Actuation Control to Improve Diesel Oxidation Catalyst Efficiency and Emissions in a Light Duty Diesel Engine. Eng. 2020;13(4561):1-26.

[34] Eastop TD, McConkey A. Applied Thermodynamics for Engineering Technologies, Fifth Edition. Pearson Education Limited, 1993.

[35] Rosli MA, Hanipah MR, Kettner M. The tuning of a small four-stroke spark ignition engine for flexible valve timings through numerical approach. MATEC Web of Conf. 2019;255(04004): 1-10.

[36] Ikpe AE, Owunna IB. Design Analysis of Reciprocating Piston for Single Cylinder Internal Combustion Engine. Int. J. Automot. Sci. Technol. 2020;4(2):30-39.

[37] Ayub A, Ayub O, Khan SA. Mathematical Modelling of In-cylinder Process in a Four Stroke Spark Ignition Engine Using MATLAB. Muhammad Ali Jinnah University, Islamabad, 2015.

[38] Hosseini AA, Ghodrat M, Moghiman M, Pourhoseini SH. Numerical study of inlet air swirl intensity effect of a Methane-Air Diffusion Flame on its combustion characteristics. Case Stu. Them. Eng. 2020;18:100610.

[39] Fatchurrohman N, Chia ST. Performance of hybrid nano-micro reinforced mg metal matrix composites brake calliper: simulation approach. IOP Conf. Series: Mat. Sci. Eng. 2017;257:1-7.

[40] Adam NM, Attia OH, Al-Sulttani O, Mahmood HA, As'arry A, Rezali KA. Numerical Analysis for Solar Panel Subjected with an External Force to Overcome Adhesive Force in Desert Areas. CFD Letts. 2020;12(9):60-75.

[41]Ramachandran S. Rapid Thermodynamic Simulation Model of an Internal Combustion Engine on Alternate Fuels. Proceedings of the International Multiconference of Engineering and Computer Scientist, 2009;2:18-20. Hong Kong.

[42] Ferguson CR, Kirkpatrick AT. Internal Combustion Engine: Applied Thermosciences, 2nd Edition, New York, John Willey and Sons, 2000.

[43] Prasad R, Samria NK. Transient Heat Transfer Analysis in Internal Combustion Engine Piston. Comp. Stru. 1990;34(5):787-793.

[44] Sharma SK, Saini PK, Samria NK. Modelling and Analysis of Radial Thermal Stresses and Temperature Field in Diesel Engine. Int. J. Eng. Sci. Tech. 2013;5(3):111-123.

[45] Descieux D, Feidt M. One Zone Thermodynamic Model Simulation of an Ignition Compression Engine. Appl. Therm. Eng. 2007;27(8-9):1457-1466.

[46] Varol Y, Oztop HF, Firat M, Koca A. CFD modeling of heat transfer and fluid flow inside a pent-roof type combustion chamber using dynamic model. Int Com. Ht. Mass Tnf. 2020;37(9): 1366-75.

[47] Ikpe AE, Bassey MO, David VO. (2023) Computation of In-Cylinder Transient Thermodynamics and Valve Lift Effects on Four Stroke Reciprocating Piston Internal Combustion Engine. Presented at the 3th International Liberty Interdisciplinary Conference, January 13-15, 2023, Miami, USA.

[48] Ikpe AE, Owunna IB. A 3D modelling of the in-cylinder combustion dynamics of two stroke internal combustion engine in its service condition. Nig. J. Tech. 2020;39(1):161-172.

[49] Pradhan R, Ramkumar P, Sreenivasan M, Sukumar P. (2012) Air-fuel Ratio (Afr) Calculation in an Internal Combustion Engine Based on the Cylinder Pressure Measurements. Int. J. Eng. Res. Appl. 2012;2(6):1378-1385.

[50] Das L, Gulati R, Gupta PK. A Comparative Evaluation of the Performance Characteristics of Spark Ignition Engine Using Hydrogen and Compressed Natural Gas as Alternative Fuel. Int. J. Hydro. Eng. 2000;25:783-793.

[51] Rahman MM, Mohammed MK, Bakar RA. Effects of Air-fuel Ratio and Engine Speed on Performance of Hydrogen Fueled Port Injection Engine. J. Appl. Sci. 2009;9(6):1128-1134.

[52] Jaaskelainen H, Khair MK. Engine Intake Charge Management. DieselNet Technology Guide. ECOpoint Inc., 2019.

[53] Iodice, P. and Cardone, M. Ethanol/Gasoline Blends as Alternative Fuel in Last Generation Spark-Ignition Engines: A Review on CO and HC Engine out Emissions. Eng. 2021;14(13): 4034.

[54] Stepien Z. A Comprehensive Overview of Hydrogen-fueled Internal Combustion Engines: Achievements and Future Challenges. Eng. 2021;14(6504):1-26.

[55] Kurniawan WH, Abdullah S, Shamsudeen A. Turbulence and heat transfer analysis of intake and compression stroke in automotive 4-stroke direct injection engine. Alg. J. Appl. Fluid Mech. 2007;1(0):37-50.

[56] Fırat M, Varol F. A Comparative Analysis of In-Cylinder Flow, Heat Transfer and Turbulence Characteristics in Different Type Combustion Chamber. Int. J. Aut. Eng. Tech. 2018;7(1):18-28.

[57] Sun T, Chang Y, Xie Z, Zhang K, Chen F, Li T, Yanet S. (2018) Experimental research on pumping losses and combustion performance in an unthrottled spark ignition engine. Proc. Inst. Mech. Engr, Part A: J. Pow. Eng, 2018;232(7): 888-897.

[58] Malkhede D, Khalane D. Maximizing Volumetric Efficiency of IC Engine through Intake Manifold Tuning. SEA Technical Paper, 2015-01-1738, 2015.

[59] Lurk AM, Och SH, Maura LM, Mariani VC, Domingues E. (2021) Maximizing Volumetric Efficiency Using Stochastic Optimization Techniques for Internal Combustion Engines. Appl. Therm. Eng. 2021;199:117603.

[60] Stone R. Introduction to internal combustion engines, 4th edition. Red Globe Press, London, 2012.

[61] Willman C, Scott B, Stone R, Richardson D. Quantitative metrics for comparison of in-cylinder velocity fields using particle image velocimetry. Exp Fluids 2020;61(62):1-16.

[62] Krishna BM, Mallikarjuna JM. Effect of Engine Speed on Cylinder Tumble Flows in a Motored Internal Combustion Engine-An Experimental Investigation Using Particle Image Velocimetry. J Appl. Fluid Mech. 2011;4(1):1-4.

[63] Khalighi B. Study of the intake Tumble Motion by Flow Visualization and Particle Tracking Velocimetry. J. Exp. Fluids, 1991;10:230-236.

[64] Heywood JB. Internal Combustion Engine Fundamentals. McGraw Hill International Editions, 1988.

[65] Hill PG, Zhang D. The effects of swirl and tumble on combustion in spark-ignition engines. Int. J. Prog. Eng. Comb. Sci. 1994;20:373-429.

[66] Raghavan KS, Pandurangadu V. Effect of Induced Turbulence in a C.I Engine by Varying Compression Ratio and Injection Timing on the Performance of the Engine. Int. J. Eng. Res. Tech. 2014;3(8):2278-0181.

[67] Eames I, Flor JB. New Development in Understanding Interfacial Process in Turbulent Flows. Phil. Tran. Ryl. Soc. 2011;369(1937):702-705.

[68] Tabaczynski RJ. Turbulent Flows in Reciprocating Internal Combustion Engines. In: Weaving J. H. (eds.) Internal Combustion Engineering: Science & Technology. Springer, Dordrecht, 243-285, 1990.

[69] El-Adawy M, Heikal MR, Aziz AR. Stereoscopic Particle Image Velocimetry Measurements and Proper Orthogonal Decomposition Analysis of the In-Cylinder Flow of Gasoline Direct Injection Engine. ASME. J. Eng. Res. Tech. 2019;141(4):042204.